

Eight luminous early-type galaxies in nearby pairs and sparse groups. I. Stellar populations spatially analysed*

D. A. Rosa^{1,2}

Divisão de Astrofísica, Instituto Nacional de Pesquisas Espaciais, São José dos Campos-SP, Brazil
Instituto de Pesquisa & Desenvolvimento, Universidade do Vale do Paraíba, São José dos Campos-SP, Brazil
deiserosa@univap.br

A. C. Milone¹

Divisão de Astrofísica, Instituto Nacional de Pesquisas Espaciais, São José dos Campos-SP, Brazil
andre.milone@inpe.br
and

A. C. Krabbe² and I. Rodrigues²

Instituto de Pesquisa & Desenvolvimento, Universidade do Vale do Paraíba, São José dos Campos-SP, Brazil
krabbe@univap.br; irapuan@univap.br

ABSTRACT

We present a detailed spatial analysis of stellar populations based on long-slit optical spectra in a sample of eight luminous early-type galaxies selected from nearby sparse groups and pairs, three of them may have interaction with another galaxy of similar mass. We have spatially measured luminosity-weighted averages of age, [M/H], [Fe/H], and $[\alpha/\text{Fe}]$ in the sample galaxies to add empirical data relative to the influence of galaxy mass, environment, interaction, and AGN feedback in their formation and evolution. The stellar population of the individual galaxies were determined through the well-established stellar population synthesis code `STARLIGHT` using semi-empirical simple stellar population models. Radial variations of luminosity-weighted means of age, [M/H], [Fe/H], and $[\alpha/\text{Fe}]$ were quantified up to half of the effective radius of each galaxy. We found trends between representative values of age, [M/H], $[\alpha/\text{Fe}]$, and the nuclear stellar velocity dispersion. There are also relations between the metallicity/age gradients and the velocity dispersion. Contributions of 1 – 4 Gyr old stellar populations were quantified in IC 5328 and NGC 6758 as well as 4 – 8 Gyr old ones in NGC 5812. Extended gas is present in IC 5328, NGC 1052, NGC 1209, and NGC 6758, and the presence of a LINER is identified in all these galaxies. The regions up to one effective radius of all galaxies are basically dominated by α -enhanced metal-rich old stellar populations likely due to rapid star formation episodes that induced efficient chemical enrichment. On average, the age and $[\alpha/\text{Fe}]$ gradients are null and the [M/H] gradients are negative, although discordant cases were found. We found no correlation between the stellar population properties and the LINER presence as well as between the stellar properties and environment or gravitational interaction, suggesting that the influence of progenitor mass can-not be discarded in the formation and evolution of early-type galaxies.

Subject headings: galaxies: elliptical and lenticular, cD galaxies: groups: general, galaxies: stellar content, galaxies: abundances, galaxies: kinematics and dynamic, galaxies: formation.

1. Introduction

The formation and evolution of elliptical and lenticular galaxies (early-type galaxies, or simply ETGs) are still open questions in Astrophysics. The modern view of formation/evolution of massive ETGs, especially ellipticals, implies a long two-phase process (Oser et al. 2010). The initial phase at high redshift is induced by dissipative fusions of small stellar systems formed through individual gravitational collapses. This initial process builds up the main body of a massive elliptical with stellar populations passively evolving such that the system rapidly turns red (Yamada et al. 2005; Zirm et al. 2008; Stark et al. 2009; Santini et al. 2009; Damjanov et al. 2011; Papovich et al. 2015; Feldmann et al. 2017). In the second phase, minor and/or major dry mergers make this main body progressively bigger and redder during many billions of years, explaining the existence of an extended stellar envelope with smaller metallicity, bluer than the nuclear region (Obreja et al. 2013; Huang et al. 2016).

Additionally, different physical mechanisms, including internal and external ones, play distinct roles in the formation and evolution of ETGs under the cold dark matter paradigm for structure formation in a Universe dominated by dark energy (Λ CDM cosmology). Some physical processes depend on the environmental conditions, such as major merging; minor merging; ram pressure, which extracts the interstellar medium; and strangulation, which strips the galactic halo (Cox 1972; Naab & Burkert 2003; van Gorkom 2004; Weinmann et al. 2009). Other physical processes are intrinsic to the galaxies themselves such as secular evolution, which modifies the internal structure; active galactic nuclei (AGN) feedback; and stellar feedback, produced by supernovae explosions (Binney & Tremaine 2008; Croton et al. 2006; Hirschmann et al. 2015). Galactic winds may interrupt the star formation by removing the gas reservoir. They can be mainly induced by the AGN feedback compared with the stellar feedback. In addition, the efficiency of galactic winds is, in some

sense, related to the galaxy gravitational potential.

While around half the galaxies in the Universe belong to groups and clusters, ETGs are less abundant in the nearby groups. Galaxy groups are a transition between clusters and field from the hierarchical point of view. They are physical entities disconnected from the cosmic expansion by mutual gravity attraction among their members, which are packed into a volume of about a few Mpc wide. Groups either hold galaxies before they are gravitationally engulfed by a cluster, or may never be captured by the gravitational potential of a cluster. Sparse groups can be gravitationally relaxed entities, especially when they hold an x-ray emitting intra-group gas. Velocity dispersion of galaxies in a group is comparable with the velocity dispersion of stars inside a galaxy (they span from 100 to 500 km s⁻¹). Consequently, encounters between two or more galaxies in a group as well as the galaxy movement inside it can play an important role for internal perturbations and perhaps galactic morphological mutation.

For the radial gradients in stellar metallicity and age classic models by Larson (1974, 1975) and Carlberg (1984a,b) show that dissipative gravitational collapse of protogalaxies with no or slow rotation produce very deep negative metallicity gradients. On the other hand, the two-phase formation process, studied by Oser et al. (2010), induces more realistic negative gradients in both metallicity and age. Mergers and strong mutual interactions are supposed to shallow these gradients by mixing the stellar populations and gas over the system (Mihos & Hernquist 1996; De Lucia et al. 2006; Sánchez-Blázquez et al. 2006b,a; Sánchez et al. 2014; Rosa et al. 2014). In fact, the gradients are strongly determined by the assembly history of the galaxy (Kobayashi 2004), and they are spatially dependent on the Star Formation History (SFH), which can also be affected by the environment.

An open question about galaxy formation is the roles played by the progenitor mass and environment for the formation/evolution of massive ETGs. This issue is the debate known as “nature versus nurture”, (e.g. Cooper et al. 2007; Tasca et al. 2009; Merlin et al. 2012). Detailed characterization of stellar populations associated or not to the ionized gas within the central region of ETGs from different nearby low-density regions provides a lot of information about the internal SFH and radial gradients of simple stellar populations. In this case, nearby massive ETGs ($z \leq$

¹Instituto Nacional de Pesquisas Espaciais (INPE), Divisão de Astrofísica, Av. dos Astronautas 1758, 12227-010, São José dos Campos-SP, Brazil

²present address: Instituto de Pesquisa & Desenvolvimento (IP&D), Universidade do Vale do Paraíba, Av. Shishima Hifumi 2911, 12244-000, São José dos Campos-SP, Brazil

0.05) are excellent physical laboratories as they can be observationally analysed in detail even with small aperture telescopes that have good instrumentation.

The current work focuses on a sample of 8 nearby luminous ETGs, in which one is an isolated galaxy and 7 are in sparse groups. Basic data on each galaxy in the sample is presented in Table 1. Six out of eight have companion galaxies that may characterize them as galaxies in pairs, according to our simple criterion (see next section), three of which are possibly in interaction. The sample also spans slow and fast rotators based on stellar kinematics measurements from the literature.

To homogeneously recover stellar population properties (age, [M/H], [Fe/H], and [α /Fe]) over the sample ETGs, we have applied the well-established spectral synthesis code *STARLIGHT* (Cid Fernandes et al. 2004, 2005; Mateus et al. 2006; Cid Fernandes et al. 2007; Asari et al. 2007). No previous work has analysed this set of ETGs based on a stellar population synthesis like we have done. Another work goal is obviously to add knowledge about formation and evolution of massive $z = 0$ ETGs from pairs and sparse groups, including interacting galaxies and LINERs.

This paper is organized as follows. Section 2 has details about the sample selection. In Section 3, we present the spectroscopic data and data reduction. The stellar population synthesis and the resulting properties are explored in Section 4, including a detailed galaxy-by-galaxy analysis (stellar content spatially resolved, radial gradients of stellar population properties and chemical enrichment at observed regions). In Section 5, all results are discussed for the ETGs sample as a whole. Finally, in Section 6, we present our conclusions.

2. The early-type galaxies sample

The observed sample of eight nearby luminous ETGs is composed of IC 5328, NGC 1052, NGC 1209, NGC 5812, NGC 6758, NGC 6861, NGC 7507, and NGC 7796. All of them are brighter than the absolute blue magnitude of the “knee” (M_B^*) of the global galaxy luminosity function at zero redshift (Liske et al. 2003; Driver & De Propris 2003), and their M_B covers almost 1 mag. Table 1 shows the global properties of the sample galaxies.

These luminous ETGs were selected to produce a sample of galaxies under possible interaction with any other galaxy. The criteria we adopted to verify

pair and group membership of a target are: **(i) sparse group:** composed by galaxies with projected linear separation of ≤ 400 kpc, and relative heliocentric radial velocity difference of ≤ 500 km s $^{-1}$; **(ii) galaxy pair:** composed of galaxies with projected linear separation of ≤ 100 kpc and heliocentric radial velocity difference of ≤ 500 km s $^{-1}$; **(iii) interacting pair:** if besides the previous criterium, it shows some signs of tidal distortion.

To apply the above criteria, we used the Physical Companions tool of NED¹ to find the group members and interacting pairs upon the standard Λ CDM cosmology ($h_0 = 0.73$, $\Omega_{\text{matter}} = 0.27$, and $\Omega_{\text{dark-energy}} = 0.73$). We also take into account the spatial scale corrected by the cosmology. The Nearby Optical Galaxy (NOG) database of Giuricin et al. (2000) was also adopted as a cross check of the environment classification if possible, because specifically IC 5328, NGC 7507, and NGC 7796 are not catalogued by NOG.

IC 5328, NGC 5812, and NGC 7507 are identified as galaxies in possible interacting pairs. NGC 1052, NGC 1209, and NGC 6861 are galaxies in weak pairs, but for all of them, signs of interactions have been reported in the past (van Gorkom et al. 1986; Sansom et al. 2000; Tal et al. 2009; Ramos Almeida et al. 2012; Tal et al. 2009; Ramos Almeida et al. 2012; Escudero et al. 2015; Machacek et al. 2010), although they currently do not have a close companion. Except for NGC 7796 (an isolated field galaxy), all the other galaxies in the sample are members of sparse groups.

Effective surface brightness μ_e , integrated visual magnitude, and structural details, such as effective radius r_e , diameter at 25 mag arcmin $^{-2}$, and apparent ellipticity ϵ (listed in Table 1), were also taken into account to fine tune selection of the targets to make the long slit spectroscopic observations possible with the chosen instrumentation (see next section). Short description of each galaxy is presented in Appendix A, showing their main relevant characteristics.

Three sample ellipticals (NGC 1052, NGC 1209, and NGC 6758) are classified as LINER hosts (Ho et al. 1997; Annibali et al. 2010; Panuzzo et al. 2011). Stellar kinematics have been measured in all sample ETGs by a myriad of previous works (Lauer

¹NASA/IPAC Extragalactic Database (NED) operated by the Jet Propulsion Laboratory, California Institute of Technology, under contract with the National Aeronautics and Space Administration; <http://ned.ipac.caltech.edu/>.

Table 1: Main characteristics and parameters of sample galaxies. ENV means environment classification. NED means NASA/IPAC Extragalactic Database. $E(B - V)_G$ is the foreground $(B - V)$ colour excess due to our Galaxy.

Galaxy ID	Morph ^[1]	ENV ^[NED]	c_{helio} ^[NED] (km/s)	m_B ^[3] (mag)	$(B - V)_e$ ^[1] (mag)	M_B ^[2] (mag)	$E(B - V)_G$ ^[4] (arcsec)	r_e ^[1] (arcsec)	r_{25} ^[1] (arcsec)	ϵ ^[1] (mag arcmin ⁻²)	μ_e ^[1] (mag)
IC 5328	E4	P, G(4)	3137	12.27	0.97	-21.00	0.013	22.2	75.4	0.3834	12.18
NGC 1052	E4	wP, G(12)	1510	11.45	1.00	-20.20	0.023	33.7	90.6	0.3082	12.15
NGC 1209	E6?	wP, G(22)	2600	12.35	1.00	-20.65	0.033	18.5	72.0	0.5214	11.83
NGC 5812	E0	P, G(6)	1970	12.19	1.03	-20.51	0.076	25.5	64.1	0.1290	12.33
NGC 6758	E+/cD?	G(7)	3404	12.61	1.05	-21.14	0.058	20.3	67.2	0.2238	12.29
NGC 6861	SA0 ^{-s}	wP, G(17)	2829	12.08	1.03	-21.14	0.048	17.7	84.6	0.3543	11.46
NGC 7507	E0	P, G(7)	1566	11.38	1.00	-20.56	0.044	30.7	82.6	0.0228	11.90
NGC 7796	E+/cD	Field	3364	12.44	1.00	-20.93	0.009	21.2	65.6	0.1290	12.20

References: [1] de Vaucouleurs et al. (1991); [2] Makarov et al. (2014); [3] Paturel et al. (2000); [4] Schlafly & Finkbeiner (2011);

Notes: In ENV column, we used P for pair with possible interaction, wP for weak pair, G for group (with the number of galaxies in parenthesis) and Field for isolated galaxies.

1985; Lauberts & Valentijn 1989; Longhetti et al. 1998; da Costa et al. 1998; Thomas et al. 2005; Idiart et al. 2007; Li et al. 2007; Ferré-Mateu et al. 2013; Baumgartner et al. 2013). The kinematical measurements in the literature enabled us to split the sample ETGs into two categories: (i) slow rotators (IC 5328, NGC 7507, and NGC 7796), and (ii) fast rotators (NGC 1052, NGC 1209, NGC 5812, NGC 6758 and NGC 6861). We dynamically classified them based on the normalized stellar kinematical anisotropy parameter $(v_{\text{rot}}^{\text{max}}/\sigma_v^0)^*$, adopting the transition between the two categories at $(v_{\text{rot}}^{\text{max}}/\sigma_v^0)^* = 0.50$, such that $(v_{\text{rot}}^{\text{max}}/\sigma_v^0)^* < 0.50$ for slow rotators and $(v_{\text{rot}}^{\text{max}}/\sigma_v^0)^* \geq 0.50$ for fast rotators.

Radial gradients of stellar populations have been empirically quantified in 6 out of 8 ETGs in our sample (Milone et al. 2007; Annibali et al. 2007; Pierce et al. 2005; Raimann et al. 2001; Rampazzo et al. 2005). Four of them were analysed by a single work (Annibali et al. 2007). IC 5328 and NGC 7507 do not have any spatial analysis of stellar population properties (age, metallicity and α -iron ratio). Annibali et al. (2007) measured luminosity-weighted averages of age, Z , and $[\alpha/\text{Fe}]$ over 7 radial apertures in NGC 1052, NGC 1209, NGC 5812, and NGC 6758 by adopting long slit spectra mainly across photometric major axis and performing a comparison of Lick indexes against simple stellar population (SSP) model predictions. They reached radial distances up to half of effective radius corrected by the ellipticity. However, no previous work had applied a detailed stellar population synthesis based on a homogeneous approach that we have done for this whole set of ETGs.

3. Observation and data reduction

Long slit spectroscopy observations of the sample galaxies were carried out with a Boller & Chivens spectrograph at the Cassegrain focus of the 1.60-m telescope of Observatório do Pico dos Dias (OPD)², which is operated by Laboratório Nacional de Astrofísica (LNA).

Stellar and galaxy spectra in the range $\lambda\lambda 4320 - 6360 \text{ \AA}$ were collected with two observing runs (one night in 1998 Oct and two nights in 1999 Aug) with a sampling of $2.01 \text{ \AA pixel}^{-1}$ by using the CCD #106 with 1024×1024 pixels (square pixel: $24 \times 24 \mu\text{m}$) and a grating of $600 \text{ lines mm}^{-1}$ (spectrograph resolving power $R = 1800$). The spectrograph slit length is 230 arcsec and its width was fixed to 2.08 arcsec for all exposures in both observing runs, i.e. slightly above the maximum value of atmospheric seeing of all observing nights (seeing denoted by $\text{FWHM}_{\text{seeing}}$), which in fact varied from 1.76 up to 2.00 arcsec. $\text{FWHM}_{\text{seeing}}$ is estimated across the spatial axis of 2-D raw spectroscopic images of standard stars (average spectroscopic flux profile at $\lambda\lambda 4320 - 6360 \text{ \AA}$), whose exposures were taken across each night. The exposure times for sample galaxies were divided in 2 or 3 integrations of 30 min each to remove cosmic ray effects and to enhance the spectrum signal-to-noise ratio (except for NGC 7507, for which we took 4 integrations of 20 min each). The spatial scale is $1.092 \text{ arcsec pixel}^{-1}$. The instrumental spectrum resolution, estimated from the broadening of isolated emission lines in the wavelength calibration spectra,

²*Based on observations carried out at the Observatório do Pico dos Dias, which is operated by the Laboratório Nacional de Astrofísica (LNA, MCTIC, Brazil).

was $\text{FWHM}_{\text{inst}} = 4.96 \pm 0.08 \text{ \AA}$ on the 1998 Oct night, $5.07 \pm 0.20 \text{ \AA}$ on the first night of 1999 Aug run, and $5.35 \pm 0.11 \text{ \AA}$ on the second night of 1999 Aug run. The average instrumental broadening of the three nights corresponds to $\sigma_{\text{inst}} = 126.5 \pm 5.0 \text{ km s}^{-1}$ at 5155 \AA . Figure 1 shows the slit position(s) for each galaxy. Table 2 gives the journal of observations. Up to three spectrophotometric standard stars were observed each night at different airmasses to provide acceptable flux calibration for the stellar population synthesis.

The spectroscopic data reduction was processed using the NOAO (National Optical Astronomical Observatory) package of IRAF³ following the usual procedures: trimming of the 2 – D raw images, bias subtraction, dark subtraction for long integrations, flat field correction, extraction of the stellar spectra, extraction of aperture spectra for each galaxy integration across the flux profile with an adequate sky level subtraction, wavelength calibration of the 1 – D spectra, flux calibration of each galaxy aperture spectrum, and averaging of each galaxy aperture spectrum with elimination of spurious noises.

The galaxy aperture spectra across the slit direction for each integration was extracted from each side of the brightness profile centre at different distances with different widths to keep decreasing the spectral signal-to-noise ratio in a low rate over the extracted spectra across the light profile (or radial distance towards the galaxy centre). In fact, the radial distances and widths of aperture spectra depend on the surface brightness distribution across the slit direction that is essentially determined by the galaxy morphology. We made a set of aperture spectrum extractions to proceed with the stellar population synthesis (see Sec. 4). We assigned an equal width for the nuclear and its two adjacent apertures (extraction width equal to 2.0 arcsec, which is the highest value of $\text{FWHM}_{\text{seeing}}$ of all nights), such that the other apertures have progressively greater widths (see Table 2 and Table 3 for IC 5328 as an example). Besides the extraction of non-concentric aperture spectra at each side of the light profile, we also extracted spectrum inside one effective radius distance, R_e^4 across the major axis direction (excepts for NGC 5812 and NGC 7507, which were done in the EW direction). The sky windows of spectral

extractions were defined at radial distances greater than R_{25} . The relative error on flux calibration is about a few percent in the flux scale (the maximum value was 6 per cent on the night of Aug 11) making the aperture spectra suitable for stellar population synthesis.

To proceed with the stellar population synthesis, we had to prepare each aperture spectrum by following two more steps: (i) de-reddening taking into account the respective Galactic line of sight extinction denoted by $E(B - V)_G$ (foreground extinction), and (ii) close transformation onto the wavelength-of-rest. Galactic extinctions and heliocentric velocities were those provided by the NED database. The second step adopted the catalogue heliocentric velocity as a first approximation associated to the heliocentric velocity correction (estimated inside IRAF), since the stellar population synthesis approach also provides a radial velocity correction, fine tuning the wavelength-of-rest calibration.

4. Stellar population synthesis

The study of stellar populations in galaxies must enable quantification or estimation of important parameters such as age, metallicity (global Z and $[M/H]$, or $[Fe/H]$ instead), and $[\alpha/Fe]$ abundance ratio that can be represented by mean values or their distributions over specific key regions of those stellar systems.

We applied the stellar population synthesis approach to obtain the spatial distribution of stellar populations in every sample galaxy. The STARLIGHT code (Cid Fernandes et al. 2004, 2005; Mateus et al. 2006; Cid Fernandes et al. 2007; Asari et al. 2007) was adopted for this purpose. In short, STARLIGHT tries to fit the observed integrated spectrum (O_λ) of a composite stellar system through a linear combination of simple stellar population spectra.

We adopted the set of semi-empirical SSP models from Vazdekis et al. (2015), with the Kroupa Universal initial mass function ($\Gamma_b = 1.30$), ranging 18 ages ($t = 0.1, 0.2, 0.3, 0.5, 0.7, 1, 2, 3, 4, 5, 6, 7, 8, 9, 10, 11, 12, \text{ and } 13 \text{ Gyr}$), six metallicities ($[M/H] = -0.96, -0.66, -0.35, 0.06, 0.26, \text{ and } 0.40$) and two α/Fe abundance ratios (0.0 and +0.4 dex). The spectral energy distributions (SEDs) of these SSPs models have reliable flux-calibrated response ($F_\lambda/L_\odot \text{ \AA}^{-1} M_\odot^{-1}$ unity, where $L_\odot = 3.826 \times 10^{33} \text{ erg s}^{-1}$). Their mid-resolution spectra (constant $\text{FWHM} = 2.51 \text{ \AA}$ or $\sigma = 64 \text{ km s}^{-1}$ at $\lambda 5000 \text{ \AA}$) cover the wavelength range

³Image Reduction and Analysis Facility, <http://iraf.noao.edu>

⁴ $R_e = r_e(1-\epsilon)^{-1/2}$ if major axis and $R_e = r_e(1+\epsilon)^{1/2}$ if minor axis, where r_e is the standard effective radius and ϵ is the apparent ellipticity, which has been corrected by the galaxy apparent ellipticity ϵ over the slit direction

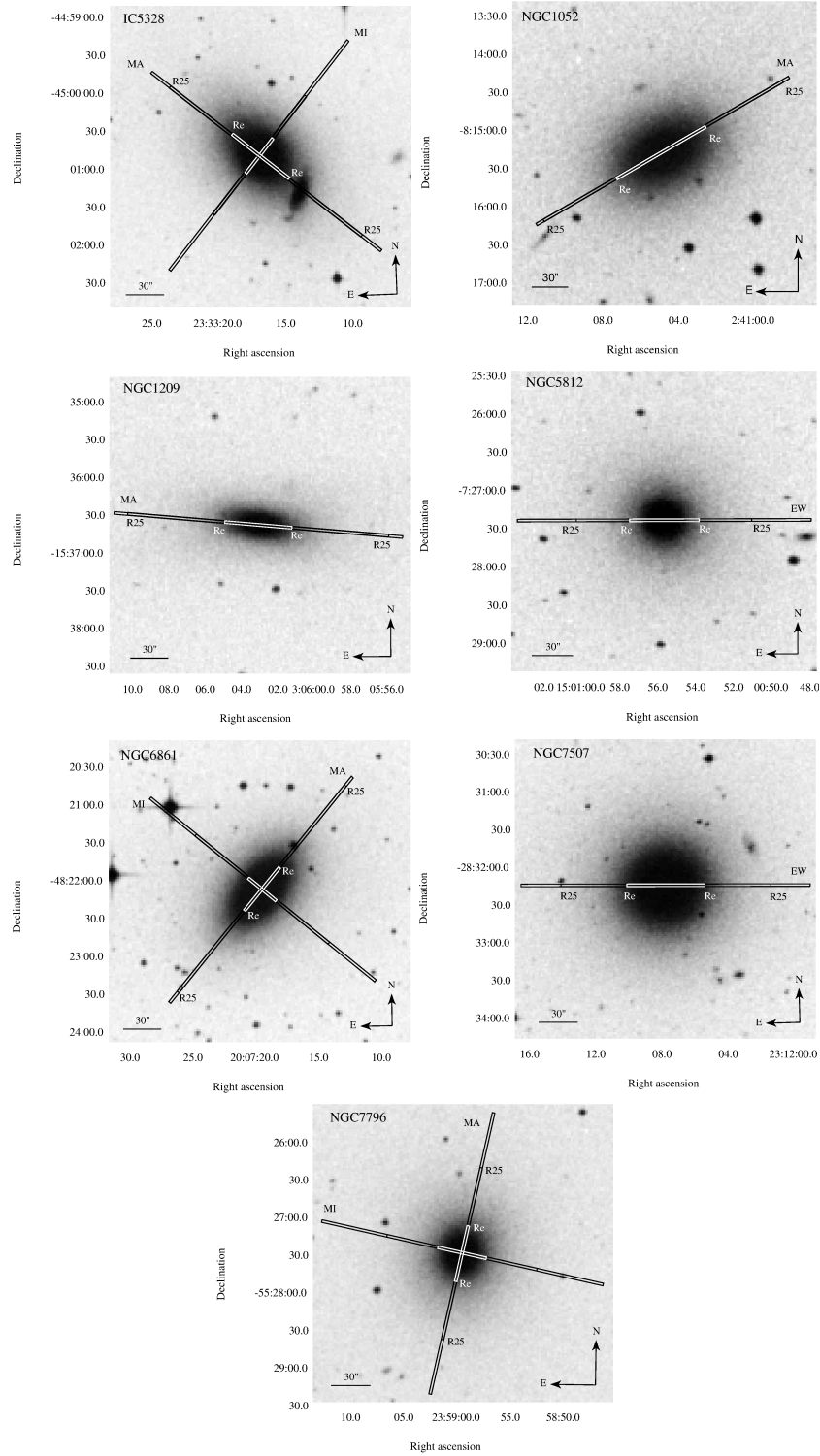


Fig. 1.— Images of our sample of galaxies with the observed slit positions. The extensions of R_c and R_{25} (both corrected by galaxy apparent ellipticity) are denoted in each optical image (IIIaJ photographic band centered at $\lambda 4680\text{\AA}$. The Digitized Sky Survey from The Space Telescope Science Institute as provided by NED, NASA/IPAC Extragalactic Database). MA means major axis direction, MI minor axis direction, and EW east-west direction.

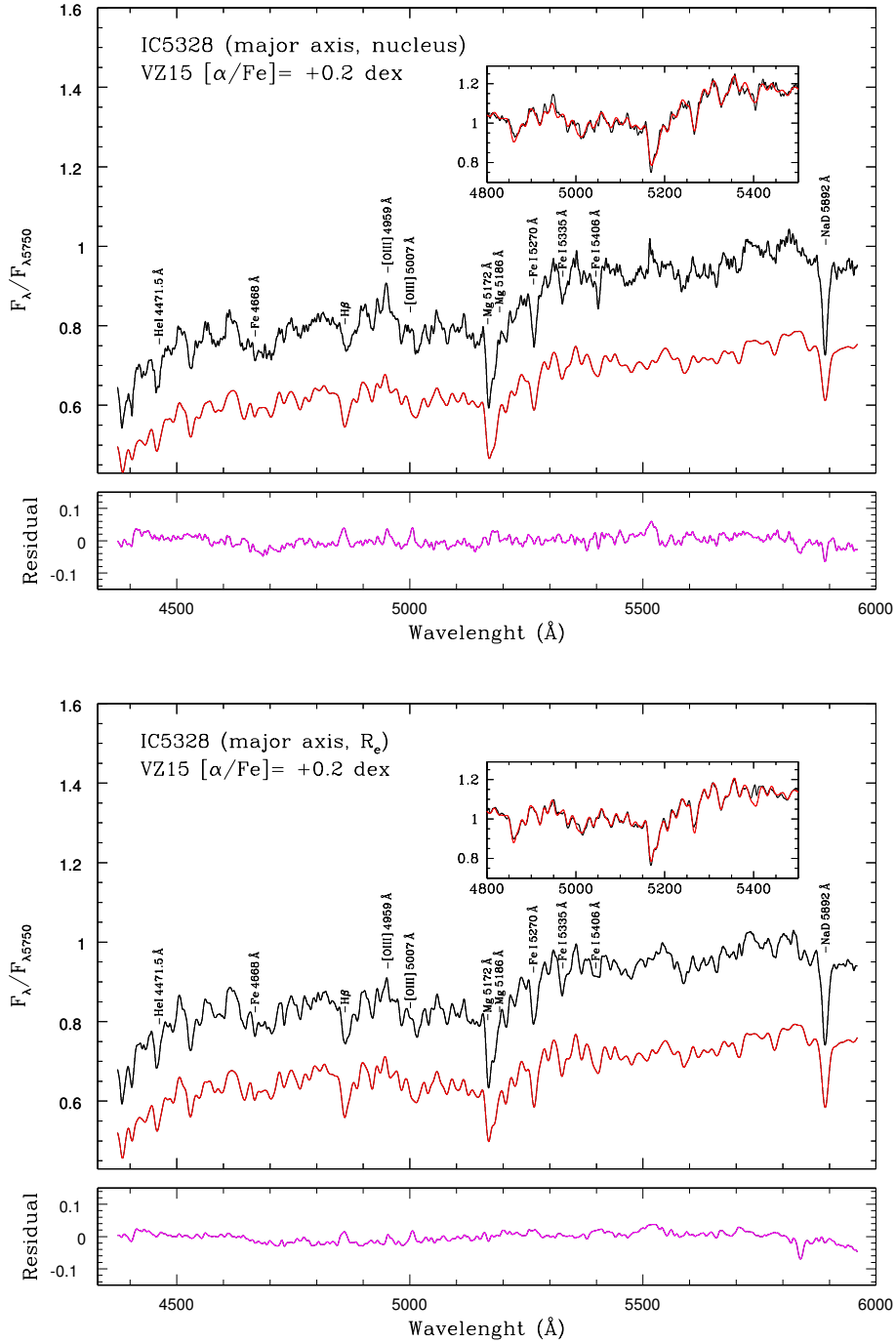


Fig. 2.— Stellar population synthesis for the nuclear and one R_e regions across the major axis of IC 5328 (left and right plots, respectively). In the top panel of each plot, the observed spectrum (in black) and the synthesized spectrum (in red) are shown. In the bottom panel, we present the flux difference between observed and synthesized spectra. The main absorption and emission features are identified in both top panels. The sub-panels illustrate the spectral fit of stellar population synthesis carried out over the spectral range used to derive $[\alpha/\text{Fe}]$ ($\lambda\lambda 4800 - 5500 \text{ \AA}$).

Table 2: Journal of observations (convention for the slit orientation according to Figure 1).

Galaxy	Date	PA _{slit}	Orientation Slit	Exposure Time	FWHM _{seeing}	Spatial Scale	R _e
		(°)		(s)	(")	(pc pix ⁻¹)	(kpc)
IC 5328	1999 August 11	40	MA	3×1800	1.91	209	5.40
	1999 August 11	130	MI	2×1800	1.79	—	3.33
NGC 1052	1999 August 12	120	MA	3×1800	2.00	93	3.44
NGC 1209	1999 August 11	85	MA	2×1800	1.91	175	4.28
NGC 5812	1999 August 12	90	EW	2×1800	1.79	156	3.65
NGC 6758	1999 August 11	121	MA	3×1800	1.76	239	5.05
	1999 August 11	211	MI	2×1800	1.91	—	3.92
NGC 6861	1999 August 12	140	MA	3×1800	1.79	193	3.56
	1999 August 12	230	MI	2×1800	1.70	—	2.52
NGC 7507	1998 August 23	90	EW	4×1200	1.91	92	2.58
NGC 7796	1999 August 12	168	MA	3×1800	1.91	229	5.77
	1999 August 12	258	MI	2×1800	2.00	—	4.15

$\lambda\lambda 3540.5 - 7409.6 \text{ \AA}$ under a sampling of 0.9 \AA .

The synthetic spectrum M_λ is solved by the STARLIGHT code according to the following equation:

$$M_\lambda = M_{\lambda_0} \left[\sum_{j=1}^{N_\star} \vec{x}_j b_{j,\lambda} r_\lambda \right] \otimes G(v_\star, \sigma_\star), \quad (1)$$

where $b_{j,\lambda}$ is the reddened spectrum of the j^{th} SSP model that is flux normalized at $\lambda_0 = 5750 \text{ \AA}$; $r_\lambda \equiv 10^{-0.4(A_\lambda - A_{\lambda_0})}$ is the extinction term; \otimes represents the convolution operator; $G(v_\star, \sigma_\star)$ is the Gaussian line of sight velocity distribution (LOSVD) centred at velocity v_\star and with a dispersion σ_\star ; M_{λ_0} is the synthetic flux at that reference wavelength; and \mathbf{x} is the stellar population vector. The stellar population vector \mathbf{x} represents the flux fractional contribution of SSPs models at λ_0 that are distributed in terms of age and metallicity (t_j, z_j). The population vector can be also expressed as a function of the SSP mass fractional contribution and is designed by the vector \mathbf{m} .

Every observed galaxy aperture spectrum O_λ is foreground de-reddened and in wavelength-of-rest. The resulting model spectrum M_λ and residual spectrum ($O_\lambda - M_\lambda$) are also in wavelength-of-rest. All of them are flux normalized at $\lambda 5750 \text{ \AA}$. M_λ and ($O_\lambda - M_\lambda$) are not corrected by the galaxy intrinsic extinction, even though A_V is estimated by the code for each galaxy aperture. The synthetic spectrum is broadened by a Gaussian function taking into account a galaxy line-of-sight velocity dispersion as estimated by the code for every aperture spectrum.

The intrinsic galactic reddening of every extracted aperture is estimated by the STARLIGHT code itself. The extinction law by Cardelli et al. (1989) is adopted (taking into account $A_V = R_V E(B - V)$ where $R_V =$

3.1), because we are dealing with early-type galaxies. See results in Table 3 specifically for IC 5328 (major axis long slit spectra only), and in the online table for the minor axis apertures of IC 5328 and other galaxies.

The STARLIGHT code provides a vector of stellar population contributions over the whole adopted SSP model grid. However, according to Cid Fernandes et al. (2005) the individual components \mathbf{x}_j are very uncertain. To troubleshoot this limitation, Cid Fernandes et al. (2005) proposed that the resulting SSP vector should be re-binned in age. In the current work, every population vector in flux contribution is represented by the following age bins or components: Young Population, f_y ($0.1 \times 10^9 < t \leq 1 \times 10^9$ years); Intermediate-young Population, f_{iy} ($1 \times 10^9 < t \leq 4 \times 10^9$ years); Intermediate-old Population, f_{io} ($4 \times 10^9 < t \leq 8 \times 10^9$ years); and Old Population, f_o ($8 \times 10^9 < t \leq 13 \times 10^9$ years), which have uncertainties lower for signal-to-noise $S/N \geq 10$ (spectral signal-to-noise ratio S/N was estimated in $\lambda\lambda 5800 - 5850 \text{ \AA}$). The same age components are employed for the SSP mass fractional contribution \mathbf{m}_j (m_y, m_{iy}, m_{io}, m_o). The quality of the resulting fit is quantified by the parameters χ^2 and *adev* (average deviation in flux). The latter gives the relative mean deviation $|(O_\lambda - M_\lambda)|/O_\lambda$ over all considered wavelengths (spectral dispersion scale binned to 1 \AA sampling as STARLIGHT works), between the observed and model spectra.

Another important issue is that a stellar population synthesis code (including STARLIGHT) does not usually provide any estimate of uncertainties for the resulting standard solution such as the luminosity-weighted average age, $[M/H]$, $[Fe/H]$, and $[\alpha/Fe]$ and their distributions (SSP output vectors). To solve this, the internal uncertainties of the parameter averages

are estimated as a function of the spectrum quality denoted by the spectral signal-to-noise ratio S/N. We performed 20 levels of random flux perturbations over every single galaxy in one R_e aperture spectrum, ran the stellar population synthesis for each perturbed spectrum, and calculated differences between the new resulting parameters and standard ones.

4.1. Spectral synthesis results

We performed the stellar population synthesis in two steps for each aperture spectrum: (i) the first one by choosing the spectral region as $\lambda\lambda 4800-5500 \text{ \AA}$, from which we just measured a unique solution of $[\alpha/\text{Fe}]$, and (ii) the second one by expanding the spectral region to $\lambda\lambda 4320-5990 \text{ \AA}$, from which we derived the definitive output SSP distributions in age and $[\text{M}/\text{H}]$ by choosing a single grid of SSPs based on the previous solution in $[\alpha/\text{Fe}]$ (the scaled-solar SSP models with $[\alpha/\text{Fe}] = 0.0$ dex or the α -enhanced SSP models with $[\alpha/\text{Fe}] = +0.4$ dex). Vazdekis et al. (2015) recommended the first spectral region to estimate $[\text{Mg}/\text{Fe}]$ (Mg is a kind of proxy for α -elements), due to the many relevant Mg- and Fe-sensitive features in there such as Mg *b* triplet, Fe I $\lambda 5015 \text{ \AA}$, Fe I $\lambda 5270 \text{ \AA}$, Fe I $\lambda 5335 \text{ \AA}$, and Fe I $\lambda 5406 \text{ \AA}$. The second region is adequately wide enough to extract information about stellar age from the spectral continuum and about stellar chemical composition from absorption features. The adopted averages of age, $[\text{M}/\text{H}]$, and $[\alpha/\text{Fe}]$ were weighted in luminosity (or flux), although we also provided the mass fractions of the SSP resulting distribution (associated to the mass fraction SSP components m_j). The flux fraction SSP components x_j , or simply the flux fraction SSP vector \mathbf{x} , were directly provided by the STARLIGHT code. The stellar population synthesis solutions in age, $[\text{M}/\text{H}]$, and $[\alpha/\text{Fe}]$ derived from both STARLIGHT steps over two different spectral regions were cross-checked between each other at every aperture spectrum. We can conclude that both solutions were in good agreement within the observational errors in the averages of age, $[\text{M}/\text{H}]$, and $[\alpha/\text{Fe}]$.

The abundance ratio $[\alpha/\text{Fe}]$ was specifically derived from three stellar population synthesis runs as proposed by Vazdekis et al. (2015): the first run adopting the scaled-solar SSP models only ($[\alpha/\text{Fe}] = 0.0$ dex), the second one with the α -enhanced SSP models only ($[\alpha/\text{Fe}] = +0.4$ dex), and the third one with all SSP models. The best solution for $[\alpha/\text{Fe}]$ is given as function of both χ^2 and a_{dev} , looking for

the minimum values of these merit figures through a second order polynomial fit (e.g. χ^2 versus $[\alpha/\text{Fe}]$) assuming $[\alpha/\text{Fe}] = +0.2$ dex for the third run. For instance, the minimum in a χ^2 fitting curve is very well located across the abscissas axis $[\alpha/\text{Fe}]$ such that the typical error that can be estimated for $[\alpha/\text{Fe}]$ is around 0.05 dex.

Afterwards we were able to estimate $[\text{Fe}/\text{H}]$ for each aperture, which was computed by taking into account a homogeneous abundance ratio relative to iron over all α -elements based on the following equation: $[\text{Fe}/\text{H}] = [\text{M}/\text{H}] - 0.75 [\text{Mg}/\text{Fe}]$, whose validity covers the ETG chemical composition (Sansom et al. 2013; Vazdekis et al. 2015). We emphasize that magnesium is assumed as a proxy of α -elements.

Figure 2 illustrates, as an example, the spectral fit of the best stellar population synthesis for both adopted spectral ranges ($\lambda\lambda 4800-5500 \text{ \AA}$ and $\lambda\lambda 4320-5990 \text{ \AA}$). This figure shows the stellar population synthesis for the nuclear and one R_e regions of IC 5328, whose spectra were extracted across its major photometric axis. Table 3 also contains as an example the resulting SSP flux (f_y , f_{iy} , f_{io} , and f_o) and mass re-binned fractions (m_y , m_{iy} , m_{io} , and m_o), age and $[\text{M}/\text{H}]$ luminosity-weighted averages, χ^2 , a_{dev} , and A_V derived from the best stellar population synthesis solution for every major axis aperture spectrum of IC 5328. The spatial variation in the contribution of the stellar population components is shown in Fig. 3 for IC 5328. Respective figures and stellar population synthesis results of other sample galaxies are in Appendix C.

The results from stellar population synthesis are separately presented galaxy-by-galaxy as follows.

4.1.1. IC 5328

The bulk of stellar populations of IC 5328 are old ($8 \times 10^9 < t \leq 13 \times 10^9$ years), reaching an average value of 88.5 per cent in light fraction and 97 per cent in mass fraction over the observed regions across its major photometric axis (see Table 3). The light and mass contributions from the intermediate-old population are negligible over all radial distances (fractions around and less than 5 per cent). There is a contribution of about 30 per cent in flux and 20 per cent in mass from the intermediate-young population at the bin $R/R_e = 0.15$ in the NE direction, as can be seen in Fig. 3. The light contribution of

Table 3: Stellar population synthesis results for all aperture spectra across the major axis of IC 5328. In the last row, we present the resulting SSP flux and mass fractions for the one R_e aperture (age re-binned as well). The results of the other seven sample galaxies and minor axis analysis of IC 5328 are available in the electronic version only.

R/R_e	Area (arcsec ²)	S/N	f_y (%)	f_{iy} (%)	f_{io} (%)	f_o (%)	m_y (%)	m_{iy} (%)	m_{io} (%)	m_o (%)	log[age] (yr)	[M/H] (dex)	χ^2	$adev$	A_V (mag)
IC 5328 MA															
-0.41SW	23.81	29	9.1	0.0	0.0	89.5	0.4	0.0	0.0	99.6	10.06	0.19	1.1	2.32	0.28
-0.25SW	14.73	48	6.5	0.0	5.9	87.6	0.3	0.0	2.1	97.6	10.04	0.20	1.2	1.95	0.26
-0.15SW	8.74	73	6.9	0.0	0.0	92.9	0.4	0.0	0.0	99.6	10.04	0.26	1.4	1.65	0.28
-0.07SW	4.16	79	6.4	2.2	0.0	90.3	0.3	0.3	0.0	99.4	10.06	0.28	1.9	1.42	0.36
0.00	4.16	92	6.3	0.0	0.0	92.3	0.3	0.0	0.0	99.7	10.07	0.37	2.3	1.34	0.49
0.07NE	4.16	76	0.0	1.8	0.0	97.3	0.0	0.4	0.0	99.6	10.09	0.22	2.0	1.41	0.25
0.15NE	8.74	78	0.0	33.1	3.4	62.9	0.0	20.3	1.4	78.4	09.98	0.30	1.5	1.69	0.08
0.25NE	14.73	66	9.3	0.0	0.0	90.8	0.3	0.0	0.0	99.7	10.07	0.22	1.1	1.84	0.22
0.41NE	23.81	26	7.5	0.0	0.0	94.1	0.6	0.0	0.0	99.4	10.09	0.16	1.1	2.20	0.18
1.00	117.73	189	10.6	0.0	0.0	88.3	0.5	0.0	0.0	99.5	10.04	0.19	2.6	0.81	0.35

the young population is always less than 10 per cent and is negligible in mass. Across the minor axis, the population synthesis found light fractions around 14 per cent by the young population at $R/R_e = 0.24$ and 0.41 (SE direction, 0.5 per cent in mass fraction) and intermediate-old at $R/R_e = 0.41$ (NW direction, 6 per cent in mass fraction). The contributions of integrated stellar populations inside one R_e indicate a predominant contribution of the old population in light fraction (around 90 per cent) as well in mass (almost 100 per cent). However, the a flux contribution is about 10 per cent for the young population. Curiously, there is no contribution from the intermediate-young population at all. In terms of chemical composition, the stellar populations are metal rich with a moderate α -enhancement. The best solutions of STARLIGHT stellar population synthesis suggest $[\alpha/Fe]= +0.14$ dex (assumed as $+0.20$ dex to run the code) for all aperture spectra. The bulk of stellar populations has $[Fe/H]= +0.25$ dex and $[M/H]= +0.40$ dex over all observed regions, reaching an average light fraction around ~ 75 per cent. The stellar population synthesis from the integrated light inside one R_e points to a global contribution of about 90 per cent for the bin $[Fe/H]= +0.25$ dex ($[M/H]= +0.40$ dex), but with also a 10 per cent of contribution for $[Fe/H]= -1.11$ dex ($[M/H]= -0.96$ dex).

4.1.2. NGC 1052

The population synthesis results in Fig. 17 indicate that the stellar light and mass across the disc of NGC 1052 (major axis direction) are mainly dominated by old stellar populations, with null or negligible contributions of the young, intermediate-

young, and intermediate-old populations over all radial distances (fractions less than ~ 5 per cent). The contributions of integrated stellar populations inside one R_e also indicate a predominant contribution of the old population in light (fraction around 89 per cent) as well in mass (fraction around 96 per cent). The residual fractions in both flux and mass contributions are due to the intermediate-old population (see specifically Fig. 17). Regarding the chemical composition, the stellar populations are metal rich with a variable α -enhancement that decreases outwards ($[M/H] \geq +0.2$ dex, $0.0 \leq [\alpha/Fe] \leq +0.4$ dex). The best solutions of population synthesis suggest $[\alpha/Fe]= 0.0$ dex for the external observed apertures, $[\alpha/Fe]= +0.2$ dex at $R/R_e = 0.10$ in both sides of the brightness profile, and $[\alpha/Fe]= +0.4$ dex for the nuclear region and two nearest apertures at $R/R_e = 0.05$ (see Fig. 17). While $[M/H]$ radially decreases outwards, $[Fe/H]$ increases from the nucleus up to $R/R_e = 0.18$ decreasing a bit from this point outwards (also see panel (a) of Fig. 4, which shows the correlated radial variations of $[M/H]$, $[Fe/H]$, and $[\alpha/Fe]$ for NGC 1052 and NGC 1209). Most stellar populations have $[Fe/H] \geq +0.10$, $+0.25$, and $+0.40$ dex (and $[M/H] \geq +0.40$ dex) over all observed regions, reaching an average light fraction around ~ 85 per cent. The stellar population synthesis from the integrated light inside one R_e points to a global contribution of about 77 per cent for the bin $[Fe/H]= +0.40$ dex ($[M/H]= +0.40$ dex), but with also a 12 per cent contribution for $[Fe/H]= -0.35$ dex ($[M/H]= -0.35$ dex), such that $[\alpha/Fe]$ curiously reaches the solar value from the best solution of population synthesis.

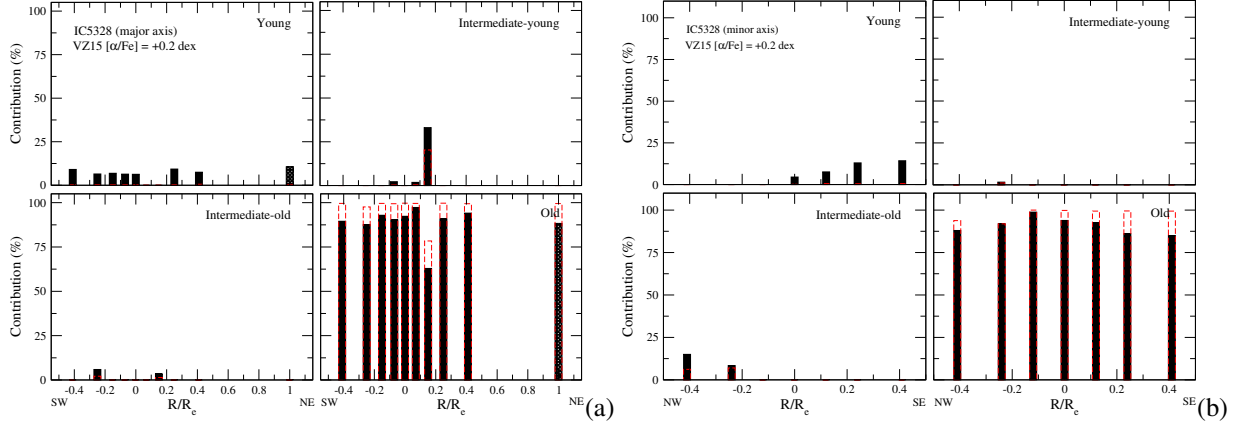


Fig. 3.— Flux and mass percental fractions (respectively black solid bars and red dashed open bars) of SSP contributions from the best solution of *STARLIGHT* population synthesis as a function of the radial distance (in R_e unity) from one side of brightness centre to other side of IC 5328 across the major (a) and minor (b) photometric axes. Each sub-panel shows the SSP flux and mass fractions in each age bin. The SSP contributions are also presented for the region inside one R_e (only derived from the major axis data analysis as shown in the top panel (a) at the farthest right bin at one R_e).

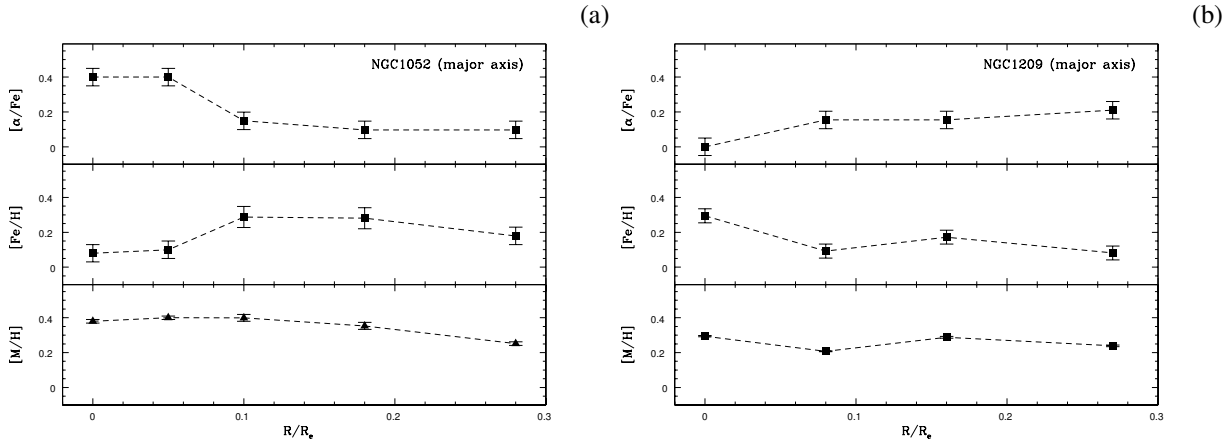


Fig. 4.— $[M/H]$, $[Fe/H]$, and $[\alpha/Fe]$ derived from the stellar population synthesis as a function of the normalized radial distance (R_e unity) for just two galaxies, NGC 1052 (panel (a)) and NGC 1209 (panel (b)), in which $[M/H]$, $[Fe/H]$, and $[\alpha/Fe]$ are correlatively variable across the major photometric axis.

4.1.3. NGC 1209

The results of the stellar population synthesis for NGC 1209 are presented in Fig. 17. NGC 1209 is light-dominated by old stellar populations, with a contribution of about ~ 86 percent in the nuclear region and higher than 91 percent in the external region towards the SW direction. The light contribution of the young population is always less than 15 percent and is negligible in mass. The contributions of integrated stellar populations inside one R_e also indicate a predominant contribution of the old population in light (fraction around 86 percent) as well in mass (fraction around 99 percent). However, there is a flux contribution of about 12 percent for the young population. The light and mass contributions from the intermediate-young and intermediate-old populations are negligible over all radial distances (fractions around and less than 5 percent). Regarding the chemical composition, the stellar populations are metal rich with a variable α -enhancement that increases outwards ($[M/H] \geq +0.2$ dex, $0.0 \leq [\alpha/Fe] \leq +0.2$ dex). The best solutions of population synthesis suggest $[\alpha/Fe] = 0.0$ dex for the nuclear region and $[\alpha/Fe] = +0.2$ dex from $R/R_e = 0.08$ outwards in both sides of the brightness profile (see Fig. 17). While $[M/H]$ is radially constant, $[Fe/H]$ decreases outwards up to $R/R_e = 0.27$ (also see panel (b) of Fig. 4). The bulk of stellar populations has $[Fe/H] \geq +0.31$ dex (and $[M/H] \geq +0.40$ dex) over all observed regions, reaching an average light fraction around ~ 74 percent. The stellar population synthesis from the integrated light inside one R_e points to a global contribution of about 78 percent for the bin $[Fe/H] = +0.25$ dex ($[M/H] = +0.40$ dex), but with also a 10 percent of contribution for $[Fe/H] = +0.11$ dex ($[M/H] = +0.26$ dex), such that $[\alpha/Fe]$ reaches over-solar value from the best solution of population synthesis.

4.1.4. NGC 5812

The majority of stellar populations of NGC 5812 is old, reaching an average value of 95 percent in percentage of light fraction and ~ 97 percent in mass fraction over the observed regions (see Fig. 17). The intermediate-old population at the nuclear region contributes to about 24 percent in flux and 21 percent in mass. The light and mass contributions from the young and intermediate-young population are negligible over all radial distances (fractions around

and less than 8 percent). The contributions of integrated stellar populations inside one R_e indicate a predominant contribution of the old population in light fraction and mass (100 percent). Curiously, intermediate-old population does not contribute in the nuclear region. In terms of chemical composition, the stellar populations are metal rich with a moderate α -enhancement. The best solutions of STARLIGHT stellar population synthesis suggest $[\alpha/Fe] = +0.2$ dex for all aperture spectra. Most of stellar populations have $[Fe/H] = +0.25$ dex and $[M/H] = +0.40$ dex over all observed regions, reaching an average light fraction around ~ 94 percent. The stellar population synthesis from the integrated light inside one R_e points to a global contribution of about 81 percent for the bin $[Fe/H] = +0.25$ dex ($[M/H] = +0.40$ dex), but with also a ~ 19 percent contribution for $[Fe/H] = +0.11$ dex ($[M/H] = +0.26$ dex).

4.1.5. NGC 6758

The population synthesis results in Fig. 17 indicate that the stellar light and mass across the disc of NGC 6758 are mainly dominated by old stellar populations, with null or negligible contributions of the intermediate-old population over all radial distances (fractions less than ~ 5 percent) across both major and minor axes. The light contribution of the young population is always less than 13 percent (major axis direction) and is negligible in mass. The intermediate-young population contributes 11 – 20 percent in flux and 6 – 9 percent in mass at the bin $R/R_e = 0.11$ in the SW direction and nuclear region across the minor axis, respectively. The contributions of integrated stellar populations inside one R_e across in the major axis direction also indicate a predominant contribution of the old population in light (fraction around ~ 94 percent) as well in mass (reaching 100 percent). In terms of chemical composition, the stellar populations are metal rich with a moderate α -enhancement. The best solutions of STARLIGHT stellar population synthesis suggest $[\alpha/Fe] = +0.2$ dex or all aperture spectra. The majority of stellar populations has ($[Fe/H] = +0.25$ dex and $[M/H] = +0.40$ dex) over all observed regions (major and minor directions), reaching an average light fraction around ~ 95 percent (see Fig. 17). The stellar population synthesis from the integrated light inside one R_e points to a global contribution of about 94 percent for the bin $[Fe/H] = +0.25$ dex ($[M/H] = +0.40$ dex), but with also 5 percent (almost negligible indeed) contribution for

[Fe/H]= -1.11 dex ([M/H]= -0.96 dex).

4.1.6. NGC 6861

The results of the stellar population synthesis for NGC 6861 are presented in Fig. 17. NGC 6861 is completely dominated by old stellar populations, marked by the contribution of both light and mass, with a contribution of nearly 100 percent over all observed regions (in both sides of the brightness profile and inside one R_e) across both major and minor axes. The light and mass contributions from the young, intermediate-young and intermediate-old population are negligible over all radial distances (fractions around and less than 5 percent). In relation to chemical composition, the stellar populations are metal rich with a high α -enhancement. The best solutions of STARLIGHT stellar population synthesis suggest $[\alpha/\text{Fe}] = +0.40$ dex for all aperture spectra. The bulk of stellar populations has [Fe/H]= $+0.10$ dex (and [M/H]= $+0.40$ dex) over all observed regions (in both sides of the brightness profile and inside one R_e), reaching an average light fraction around ~ 99 per cent.

4.1.7. NGC 7507

Most of the stellar populations of NGC 6861 are old, reaching an average value of almost 100 percent in percentage of light and mass fractions over the observed regions across the slit position. (see Fig. 17). The contributions of integrated stellar populations inside one R_e also indicate a predominant contribution of the old population in light (fraction around 90 percent) as well as in mass (fraction around 97 percent), but also including a contribution of 9 per cent in light fraction by a young population. The light and mass contributions from the young, intermediate-young, and intermediate-old populations are negligible over all radial distances (fractions around and less than 8 percent). Regarding the chemical composition, the stellar populations are metal rich with a moderate α -enhancement. The best solutions of STARLIGHT stellar population synthesis suggest $[\alpha/\text{Fe}] = +0.2$ dex for all aperture spectra. The bulk of stellar populations has [Fe/H]= $+0.25$ dex (and [M/H]= $+0.40$ dex) over all observed regions, reaching an average light fraction around ~ 84 percent. The stellar population synthesis from the integrated light inside one R_e points to a global contribution of about 86 percent for the bin [Fe/H]= $+0.25$ dex ([M/H]= $+0.40$ dex), but with

small contributions at the bins [M/H] = -0.96 , -0.66 , and -0.35 dex (almost negligible indeed).

4.1.8. NGC 7796

In Fig. 17, the population synthesis results indicate that the stellar light and mass across the disc of NGC 7796 are mainly dominated by old stellar populations, with null or negligible contributions of the young, intermediate-young, and intermediate-old populations (fractions less than ~ 5 percent) over all radial distances of the observed regions across both major and minor axes. The stellar populations are metal rich with a moderate α -enhancement for all aperture spectra (best solutions give $[\alpha/\text{Fe}] = +0.2$ dex). The bulk of stellar populations has [Fe/H]= $+0.25$ dex (and [M/H]= $+0.40$ dex) over all observed regions (in both sides of the brightness profile and inside one R_e), reaching an average light fraction around ~ 97 percent.

4.2. Radial gradients of the stellar population properties

By compiling the results of STARLIGHT stellar population synthesis for all aperture spectra of every sample galaxy, we obtained the spatial distributions of luminosity-weighted average age, [M/H], and $[\alpha/\text{Fe}]$ across the observed slit directions. For this, we computed radial gradients of age and [M/H], expressed by $(\Delta(\log(\text{age}))/\Delta(R/R_e))$ and $(\Delta([\text{M}/\text{H}])/\Delta(R/R_e))$, respectively. These gradients are also used to estimate the values at $R = 0$ of age and global metallicity. Table 4 lists these results. Figures 5-8 show age and [M/H] as a function of the normalized radial distance (in R_e unity) for all sample galaxies, in which we also present the linear *lsq* fit. A two-sigma clipping is applied on these fits, in which the outliers are designed as open symbols. Table 5 compiles the stellar parameters derived from the stellar population synthesis (nuclear and R_e integrated values of age, [M/H], $[\alpha/\text{Fe}]$, [Fe/H]). In Appendix B, the results about the radial gradients of stellar population properties are presented galaxy-by-galaxy.

The radial age and metallicity gradients, measured up to $0.15 - 0.40 R/R_e$ from the STARLIGHT stellar population synthesis, indicate that the stellar populations are evolved, metal rich, and α -enhanced. The stellar age is radially uniform over the observed regions reaching a value around $12 - 13$ Gyr (except in NGC 7507, for which we measured 10 Gyr). The

Table 4: Radial gradients of two stellar population syntheses resulting in parameters for sample galaxies: age ($\Delta(\log(\text{age}))/\Delta(R/R_e)$) and global metallicity ($\Delta([M/H])/R/R_e$) with their errors. The nuclear values of age and $[M/H]$ are also showed. The values of both parameters are light-weighted means. Means and standard deviations of gradients and nuclear values of age and metallicity are shown in the last two rows (data taken along the EW direction are considered in the mean computations of both major and minor axis directions).

galaxy ID	slit direction	age		$[M/H]$	
		gradient [dex/(R/R_e)]	age ($R/R_e = 0$) [Gyr]	gradient [dex/(R/R_e)]	$[M/H]$ ($R/R_e = 0$) [dex]
IC 5328	MA	$+0.01 \pm 0.05$	12 ± 1	-0.36 ± 0.10	0.32 ± 0.02
IC 5328	MI	-0.13 ± 0.07	12 ± 1	-0.52 ± 0.19	0.33 ± 0.05
NGC 1052	MA	-0.11 ± 0.03	13 ± 1	-0.79 ± 0.22	0.42 ± 0.04
NGC 1209	MA	$+0.11 \pm 0.11$	11 ± 1	-0.14 ± 0.18	0.27 ± 0.03
NGC 5812	EW	-0.18 ± 0.07	14 ± 1	-0.25 ± 0.15	0.41 ± 0.03
NGC 6758	MA	-0.04 ± 0.10	12 ± 1	-0.25 ± 0.14	0.40 ± 0.03
NGC 6758	MI	$+0.06 \pm 0.14$	12 ± 1	-0.15 ± 0.11	0.39 ± 0.02
NGC 6861	MA	$+0.02 \pm 0.02$	13 ± 1	-0.01 ± 0.01	0.40 ± 0.00
NGC 6861	MI	$+0.05 \pm 0.03$	13 ± 1	$+0.16 \pm 0.10$	0.36 ± 0.02
NGC 7507	EW	$+0.08 \pm 0.13$	12 ± 1	-0.46 ± 0.39	0.41 ± 0.04
NGC 7796	MA	-0.02 ± 0.02	13 ± 1	-0.08 ± 0.05	0.40 ± 0.01
NGC 7796	MI	$+0.01 \pm 0.01$	13 ± 1	$+0.01 \pm 0.01$	0.40 ± 0.00
Means	MA/EW	-0.02 ± 0.10	13 ± 1	-0.29 ± 0.25	0.39 ± 0.05
Means	MI/EW	-0.02 ± 0.11	13 ± 1	-0.20 ± 0.26	0.38 ± 0.03

Table 5: Luminosity-weighted means of age, $[M/H]$, $[Fe/H]$, and $[\alpha/Fe]$ as directly estimated by the stellar population synthesis for the apertures of nucleus ($r \leq 1$ arcsec) and one R_e corrected by ellipticity ($r \leq R_e$).

galaxy ID	age_{mean}		$[M/H]_{\text{mean}}$		$[Fe/H]_{\text{mean}}$		$[\alpha/Fe]_{\text{mean}}$	
	nucleus	$r \leq R_e$	nucleus	$r \leq R_e$	nucleus	$r \leq R_e$	nucleus	$r \leq R_e$
IC 5328	12 ± 1	11 ± 1	$+0.37 \pm 0.01$	$+0.19 \pm 0.01$	$+0.27 \pm 0.05$	$+0.09 \pm 0.04$	$+0.14 \pm 0.05$	$+0.14 \pm 0.05$
NGC 1052	13 ± 1	12 ± 1	$+0.38 \pm 0.01$	$+0.25 \pm 0.01$	$+0.08 \pm 0.05$	$+0.25 \pm 0.04$	$+0.40 \pm 0.05$	$+0.00 \pm 0.05$
NGC 1209	10 ± 1	10 ± 1	$+0.295 \pm 0.004$	$+0.273 \pm 0.003$	$+0.29 \pm 0.04$	$+0.12 \pm 0.04$	$+0.00 \pm 0.05$	$+0.21 \pm 0.05$
NGC 5812	10 ± 1	13 ± 1	$+0.40 \pm 0.01$	$+0.37 \pm 0.01$	$+0.30 \pm 0.05$	$+0.20 \pm 0.05$	$+0.13 \pm 0.05$	$+0.23 \pm 0.05$
NGC 6758	10 ± 1	11 ± 1	$+0.40 \pm 0.01$	$+0.32 \pm 0.004$	$+0.30 \pm 0.05$	$+0.22 \pm 0.04$	$+0.14 \pm 0.05$	$+0.14 \pm 0.05$
NGC 6861	12 ± 1	13 ± 1	$+0.40 \pm 0.01$	$+0.38 \pm 0.01$	$+0.10 \pm 0.05$	$+0.08 \pm 0.04$	$+0.40 \pm 0.05$	$+0.40 \pm 0.05$
NGC 7507	11 ± 1	10 ± 1	$+0.39 \pm 0.01$	$+0.29 \pm 0.01$	$+0.29 \pm 0.05$	$+0.19 \pm 0.05$	$+0.13 \pm 0.05$	$+0.13 \pm 0.05$
NGC 7796	13 ± 1	13 ± 1	$+0.394 \pm 0.003$	$+0.394 \pm 0.001$	$+0.31 \pm 0.04$	$+0.27 \pm 0.04$	$+0.11 \pm 0.05$	$+0.17 \pm 0.05$

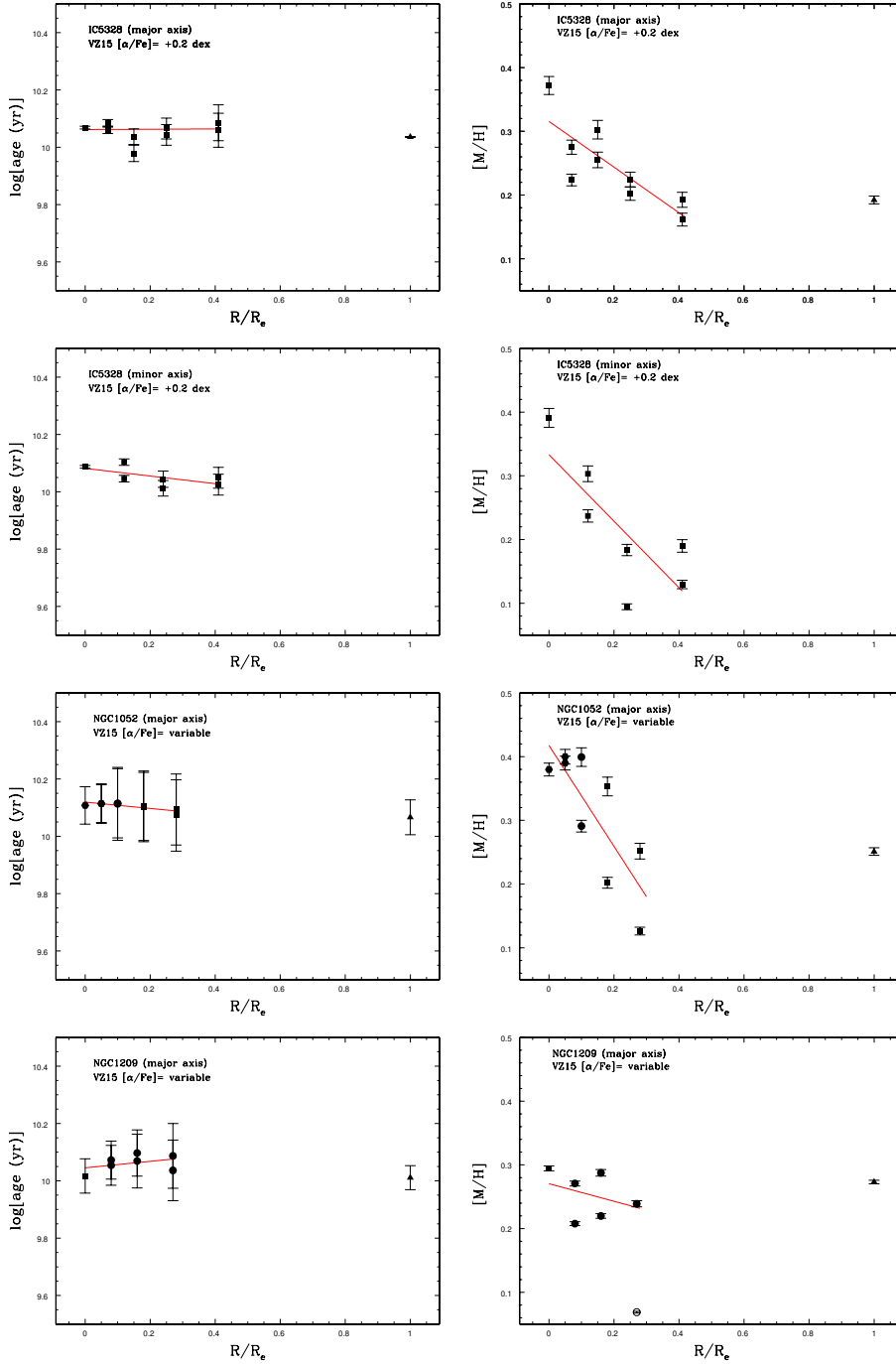


Fig. 5.— Luminosity-weighted means of age and $[M/H]$ derived from the stellar population synthesis as a function of the normalized radial distance (R_e unity), for IC 5328, NGC 1052, and NGC 1209. The direction, across which these resulting parameters were derived, is also indicated after the galaxy name (top left corner). The applied *lsq* linear fit with two sigma clipping is represented by a red line to derive the respective radial gradients of age and $[M/H]$. The triangles represent the regions of one R_e . The outlier points are assigned by open symbols. The results for NGC 5812 and NGC 7507 have been derived across the east-west direction only.

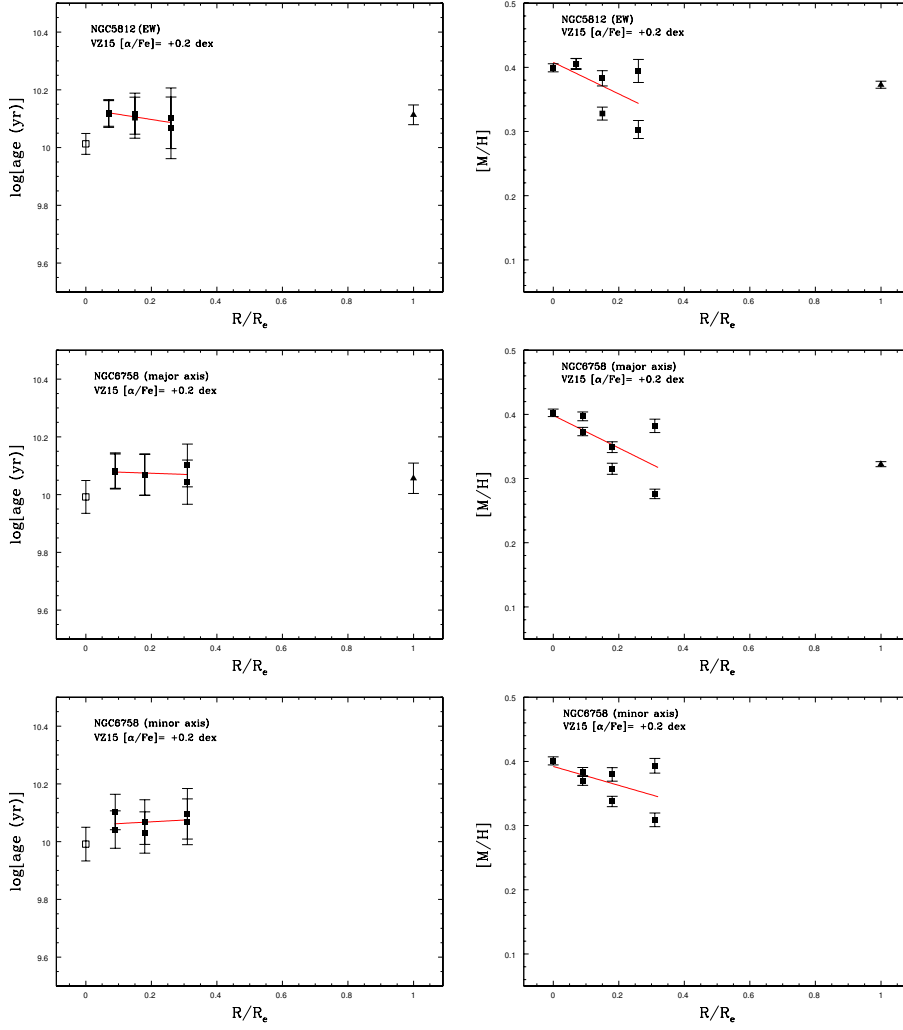


Fig. 6.— Same as Fig. 5, but for NGC 5812 and NGC 6758 as indicated.

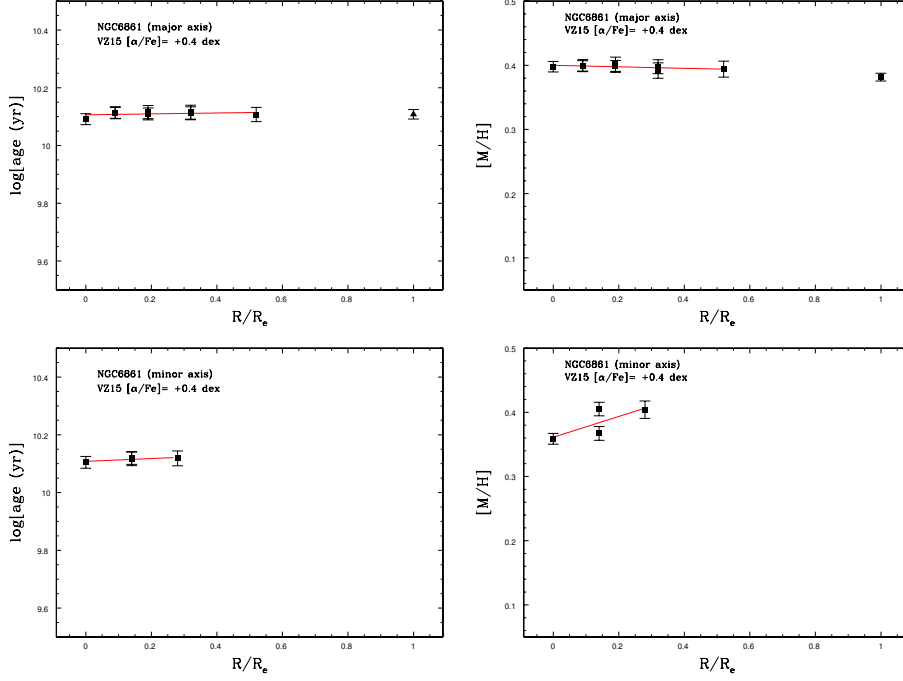


Fig. 7.— Same as Fig. 5, but for NGC 6861.

stellar total metallicity exhibits a negative radial gradient in IC 5328, NGC 1052, NGC 5812, and NGC 7507, for which the variations in $[M/H]$ are many times greater than its typical error; a flat gradient in NGC 1209, NGC 6758, and NGC 7796; and a positive gradient over the minor axis only of NGC 6861, for which the variation in $[M/H]$ is curiously three times greater than its typical error. For $[\alpha/Fe]$, our stellar population synthesis results denote an over-solar value for the majority of sample galaxies such that some have a constant α -enhancement (IC 5328, NGC 5812, NGC 6758, NGC 7507, and NGC 7796 with $[\alpha/Fe]= +0.2$ dex and NGC 6861 with $+0.4$ dex). Only two galaxies have variable α -enhancement: NGC 1052 with a high negative gradient and NGC 1209 with a moderate positive gradient. In terms of the radial variation in $[Fe/H]$, IC 5328, NGC 1209, NGC 5812, and NGC 7507 have a negative gradient; NGC 6758 and NGC 7796 have a constant value; NGC 1052 has a positive gradient; and NGC 6861 has a positive gradient over the minor axis only and a constant value over the major axis.

4.3. Chemical enrichment in observed regions of the sample galaxies

With the results from the stellar population synthesis, we were also able to investigate the relation between age and metallicity measured over different radial distances to obtain an overall picture of the chemical enrichment in the region inside one R_e of each galaxy as traced by the spatial distribution of stellar populations properties. Figure 9 shows the luminosity-weighted average global metallicity $[M/H]$ as a function of luminosity-weighted average age for two sample galaxies as an example (NGC 1052 and NGC 1209), by splitting the observed region of each galaxy up to five radius bins: $r \leq 1$ arcsec (assumed as galactic nucleus for all objects), $r \sim 0.1 R_e$, $r \sim 0.2 R_e$, $r \sim 0.3 R_e$, and $r \sim 0.4 R_e$. These two galaxies exhibit distinct chemical enrichments between each other. The uncertainties in age and $[M/H]$ of each aperture are estimated as a function of the spectral S/N. Age and metallicity of radially symmetric apertures are averaged. The integrated age and metallicity measured inside one R_e are also presented on the plot $[M/H]$ vs. age. These stellar population parameters are separately shown, galaxy by galaxy, on similar plots of Fig. 18 of Appendix C. The

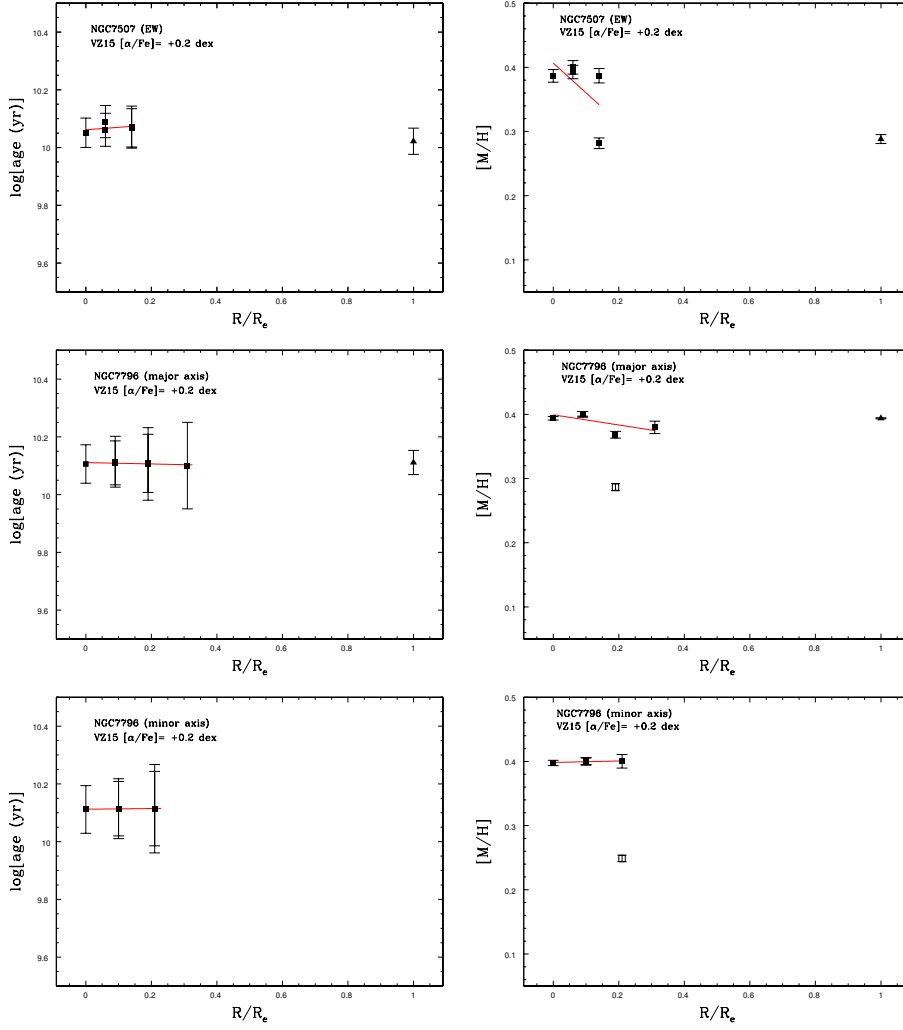


Fig. 8.— Same as Fig. 5, but for NGC 7507 and NGC 7796.

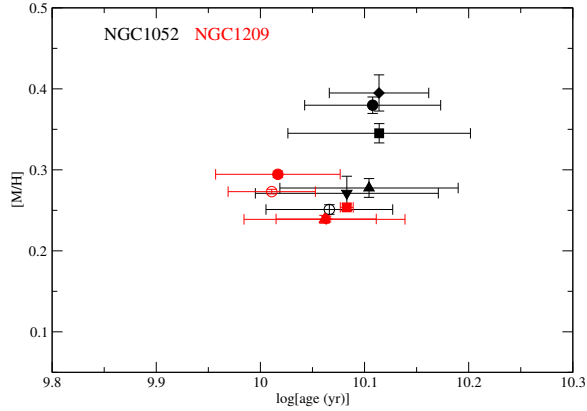


Fig. 9.— Luminosity-weighted average global metallicity $[M/H]$ as a function of luminosity-weighted average age as derived from the *STARLIGHT* stellar population synthesis in different observed radial distances for NGC 1052 and NGC 1209 across major axis. Different radial distances are assigned distinct symbols: (i) nuclear region is represented by filled circles; (ii) the closest apertures to the nucleus $r \sim 0.1 R_e$ by filled diamonds; (iii) the region $r \sim 0.2 R_e$ by filled squares; (iv) the region $r \sim 0.3 R_e$ by pointed side up filled triangles; (v) the region $r \sim 0.4 R_e$ by upside down filled triangle; and (vi) the integrated region inside $1 R_e$ by an open circle.

possible relations between age and metallicity over the observed radial distances are individually analysed in the following paragraphs.

For NGC 1052, there is a narrow radial trend between the global metallicity and age suggesting a well-defined spatial history for the chemical enrichment that correlates four parameters among each other (age, global metallicity, iron abundance, and alpha enrichment). Although the star formation occurred in a relative short time-scale (~ 1 Gyr), it seems to have been through an inside-out process that induced a decrease of global metallicity (always over-solar) together with a decrease of $[\alpha/Fe]$ and an increase of iron abundance (major axis direction); see also Fig. 4. The integrated age and metallicity inside one R_e are very close to the data of other observed apertures.

The case of NGC 1209 is in some sense unique. It has a very weak radial tendency between global metallicity and age that can be marginally suggested despite the spatially homogeneous old age and over-solar global metallicity. $[M/H]$ is weakly anti-correlated with age such that the stars in the nucleus seem to have been formed just after the stars in the external regions (a kind of outside-in process) that could explain the inward decrease of $[\alpha/Fe]$ associated with the inward increase of $[Fe/H]$ (see also Fig. 4). The integrated age and metallicity inside one R_e are very close to the data of other observed apertures.

The time-scale of star formation in IC 5328 was very short as indicated by the small spread in age (~ 1 Gyr), which can be associated to the spatially uniform and moderate $[\alpha/Fe]$ ($+0.2$ dex). We also measured a decrease of global metallicity of around 1 dex ($[M/H]$ scales) from the nucleus up to $r \sim 0.4 R_e$ during this time-scale (major axis direction). The integrated age and metallicity inside one R_e are a kind of mean over all observed apertures.

The cases of NGC 5812, NGC 6758, NGC 6861, NGC 7507, and NGC 7796 are quite similar. The lack of correlation between over-solar global metallicity and old age indicates a rapid star formation with a strong and fast chemical enrichment. We measured a spatially homogeneous α -enhancement for all of them: moderate in NGC 5812, NGC 6758, and NGC 7507 ($[\alpha/Fe] = +0.2$ dex), and high in NGC 6861 ($[\alpha/Fe] = +0.4$ dex). The integrated age and metallicity inside one R_e are very close to the data of other observed apertures in every galaxy.

In the following paragraphs, we compile our analysis relative to the stellar content against other literature works in a galaxy-by-galaxy base.

IC 5328. The integrated stellar populations inside one R_e of this galaxy are 90 per cent old ($8 \text{ Gyr} < t \leq 13 \text{ Gyr}$) and 10 per cent young ($100 \text{ Myr} < t \leq 1 \text{ Gyr}$) with an average age of 11 Gyr (light-weighted mean age) and also metal rich (light-

weighted means of $[M/H]= +0.19$ dex, $[Fe/H]= +0.09$ dex, and $[\alpha/Fe]= +0.14$ dex). The respective stellar population contributions in mass for age are 99.5 per cent (old) and 0.5 per cent (young). There are negative radial gradients of $[M/H]$ and $[Fe/H]$ associated to a homogeneous moderate α -enhancement ($[\alpha/Fe]= +0.14$ dex). Specifically, we found a light fraction contribution of 33 per cent (20 per cent in mass fraction) from an intermediate-young stellar population ($1 \text{ Gyr} < t \leq 4 \text{ Gyr}$) at $r = 0.15 R_e$ in the NE direction (major axis slit direction). Across the minor axis, the population synthesis revealed light fractions around 14 per cent by a young population at $R/R_e = 0.24$ and 0.41 (SE direction, 0.5 per cent in mass fraction) and intermediate-old at $R/R_e = 0.41$ (NW direction, 6 per cent in mass fraction). Except for $[\alpha/Fe]$, the estimates of age and $[Fe/H]$ at nucleus by Terlevich & Forbes (2002) ($R_e/8$) do not agree with our measured light-weighted means (12 Gyr, $[M/H]= +0.37$ dex, $[Fe/H]= +0.27$ dex, and $[\alpha/Fe]= +0.14$ dex). The current work was the first to measure the radial gradients of stellar population properties for this galaxy. As perspective, we could investigate whether there is a relation between the presence of young/intermediate-young populations and the nuclear gas emission.

NGC 1052. The integrated stellar populations within one R_e for this object are 12 Gyr old and have $[M/H]= +0.25$, $[Fe/H]= +0.25$, and $[\alpha/Fe]= 0.00$ dex (light-weighted means). The radial gradients measured up to about $0.3 R_e$ are negatively steep in $[M/H]$ and $[\alpha/Fe]$ (outward variations of -0.24 dex and -0.4 dex respectively), associated with a positive gradient in $[Fe/H]$ ($+0.2$ dex of outward increase). Age shows a shallow negative gradient (variation of only -1 Gyr). Our measurements of stellar population properties in the nuclear region of **NGC 1052** corroborate previous estimates, for example, those by Annibali et al. (2007) for the $R_e/8$ aperture. We speculate that the AGN activity in this elliptical may have been strong in the past to quench the star formation in the nucleus and to justify the great nuclear α -enhancement ($[\alpha/Fe]= 0.40$ dex) that rapidly decreases outwards, as also identified by Milone et al. (2007) based on comparison of Lick indices against SSP models. The radial decrease of $[\alpha/Fe]$ and increase of $[Fe/H]$ across the major axis might be explained by an inside-out star formation process.

NGC 1209. The integrated stellar populations

within one R_e of this galaxy are 10 Gyr old and have $[M/H]= +0.27$ dex, $[Fe/H]= +0.25$ dex, and $[\alpha/Fe]= 0.00$ dex (light-weighted means). The radial gradient, measured up to about $0.3 R_e$, is negative in $[Fe/H]$ and positive in $[\alpha/Fe]$ (outward variation of -0.2 dex and $+0.2$ dex respectively from $r = 0$), associated with a null gradient in $[M/H]$. Age does not show any change. Our measurements of total metallicity $[M/H]$ in the nuclear region of **NGC 1209** agree with Annibali et al. (2007) ($R_e/8$ aperture), but our age quantification differs from their estimate by 5 Gyr. Other previous investigations obtained some contradictory results. On the one hand, Terlevich & Forbes (2002), by analysing high quality line index data, derived stellar populations with mean age around 15 Gyr and solar metallicity $[Fe/H]= -0.01$ dex. Howell (2005) found that old metal-rich populations dominate the nucleus (age= 15.6 Gyr, $[Z/H]= +0.28$ dex, $[\alpha/Fe]= 0.23$ dex). On the other hand, Idiart et al. (2007), by applying parametric calibrations of Lick indexes, concluded that the mean stellar population age in NGC 1209 is about 9.3 Gyr associated to an over-solar metallicity. The radial distribution of stellar populations in this galaxy is indeed peculiar. This behaviour could be due to an outside-in star formation process, which would explain the gradual decrease of α -enhancement inwards.

NGC 5812. The integrated stellar populations within one R_e of this object are 13 Gyr old and have $[M/H]= +0.37$ dex, $[Fe/H]= +0.20$ dex, and $[\alpha/Fe]= +0.23$ dex (light-weighted means). The radial gradient, measured up to about $0.3 R_e$, is slightly negative in age (outward variation of -1 Gyr from $r = 0$), negative in $[M/H]$ (variation of -0.07 dex outwards from $r = 0$), and positive in $[Fe/H]$ (variation of $+0.07$ dex outwards from $r = 0$). There is no variation in $[\alpha/Fe]$. Only in the nuclear region ($r \leq 1$ arcsec), the stellar population synthesis revealed a contribution of 24 per cent in flux fraction (20 per cent in mass fraction) by an intermediate-old population ($4 \text{ Gyr} < t \leq 8 \text{ Gyr}$), such that the light-weighted age reaches a smaller value of 10 Gyr. Our results in stellar population properties agree quite well with those measured by Annibali et al. (2007) for the $R_e/8$, but marginally for age (8.5 Gyr was their estimate). The stellar content of NGC 5812 has also been analysed by some works (Trager et al. 2000b,a; Thomas et al. 2005; Sánchez-Blázquez et al. 2006b; Annibali et al. 2007; Ferré-Mateu et al. 2013). However, the nuclear aperture is excluded to compute the age gradient by a two σ clipping, which is why

the age gradient is estimated as negative. If this intermediate-old age contribution is real, some more extended star formation could have occurred in this ETG, which would justify its homogeneous moderate α -enhancement ($[\alpha/\text{Fe}] = +0.2$ dex).

NGC 6758. The integrated stellar populations within one R_e of this galaxy are 11 Gyr old and have $[\text{M}/\text{H}] = +0.32$ dex, $[\text{Fe}/\text{H}] = +0.20$ dex, and $[\alpha/\text{Fe}] = +0.14$ dex (light-weighted means). There is no radial gradient in age, as measured up to about $0.3 R_e$. The gradient is negative in $[\text{M}/\text{H}]$ (variation of -0.15 dex outwards from $r = 0$) and positive in $[\text{Fe}/\text{H}]$ (variation of $+0.15$ dex outwards from $r = 0$). A moderate α -enhancement ($[\alpha/\text{Fe}] = +0.14$ dex) is radially constant. Just in the nuclear aperture of minor axis exposure, the stellar population synthesis indicated a contribution of 19 per cent in flux fraction (or 9 per cent in mass fraction) by an intermediate-young population, 4 per cent by an intermediate-old population and 77 per cent in flux fraction by an old population. The major axis of the nuclear aperture provides a contribution of 6 per cent in flux fraction (or 3 per cent in mass fraction) by this intermediate-young population and 94 per cent in flux fraction by an old population. Our results in stellar population properties compared with those measured by Annibali et al. (2007) for the $R_e/8$ only agree marginal because they estimated 16 Gyr, solar metallicity, and a greater α -enhancement ($[\alpha/\text{Fe}] = +0.32$ dex). Annibali et al. (2007), for instance, measured for the $R_e/8$ aperture, as luminosity-weighted average stellar population properties, an extremely old age (16.0 ± 2.5 Gyr), a solar metallicity ($Z = 0.016 \pm 0.002$), and an over-solar α/Fe ratio ($[\alpha/\text{Fe}] = +0.32 \pm 0.05$ dex). If the contribution of an intermediate-young population at the centre is actually valid, a long star formation process could have occurred in this ETG nuclei, which would justify its homogeneous moderate α -enhancement ($[\alpha/\text{Fe}] = +0.14$ dex).

NGC 6861. For this galaxy the integrated stellar populations within one R_e are 13 Gyr old and have $[\text{M}/\text{H}] = +0.38$ dex, $[\text{Fe}/\text{H}] = +0.08$ dex, and $[\alpha/\text{Fe}] = +0.40$ dex (light-weighted means). All gradients in stellar population properties (age, $[\text{M}/\text{H}]$, $[\text{Fe}/\text{H}]$, $[\alpha/\text{Fe}]$) are consistent with zero. Our results from the stellar population synthesis agree with those estimated by Raimann et al. (2001, 2005), who stated that representative stellar population properties should be measured at $r = r_e$. The stars in this ETGs must have been formed very fast through efficient star formation

episode(s) before the system mass assembly, despite the existence of stellar rotating disc that could have involved some energy dissipation and/or could have been formed by a secular process.

NGC 7507. Its integrated stellar populations within one R_e are 10 Gyr old and have $[\text{M}/\text{H}] = +0.29$ dex, $[\text{Fe}/\text{H}] = +0.19$ dex, and $[\alpha/\text{Fe}] = +0.13$ dex (light-weighted means). The globally a contribution by young population is 9 per cent in light fraction. Li et al. (2007) found a shorter age (4 Gyr), but the over-solar metallicity measured by them is in agreement with our estimate. The current work was the first that measured the radial gradients of stellar population properties for this galaxy. There is no radial gradient in age, as measured up to about $0.15 R_e$. The gradient is negative in $[\text{M}/\text{H}]$ (variation of -0.07 dex outwards from $r = 0$) and positive in $[\text{Fe}/\text{H}]$ (variation of $+0.07$ dex outwards from $r = 0$). A moderate α -enhancement ($[\alpha/\text{Fe}] = +0.13$ dex) is radially constant. The bulk of stars in this ETG nuclei must have been formed under an efficient process, but a young population has a small contribution (negligible in mass fraction), which could be related to some star formation induced by the fusion of two spirals involving such a small gas mass.

NGC 7796. Its integrated stellar populations within one R_e are 13 Gyr old and have $[\text{M}/\text{H}] = +0.39$ dex, $[\text{Fe}/\text{H}] = +0.27$ dex, and $[\alpha/\text{Fe}] = +0.17$ dex (light-weighted means). The current work was the first to measure the radial gradients of stellar population properties for this galaxy. All gradients in stellar population properties (age, $[\text{M}/\text{H}]$, $[\text{Fe}/\text{H}]$, $[\alpha/\text{Fe}]$) are consistent with zero (radial distance up to about $0.35 R_e$). Thomas et al. (2005) and Milone et al. (2007) had estimated old age and metal rich populations for this ETG. However, Milone et al. (2007) wrongly suggested negative gradients in age, total metallicity, and $[\alpha/\text{Fe}]$. The stars in this ETGs must have been formed very fast through efficient star formation episode(s) before the system mass assembly.

4.4. Warm ionized gas detection in five sample galaxies

We detected emission lines for five galaxies of our sample after the subtracting of the underlying stellar population spectrum, which was derived from the stellar population synthesis. For IC 5328, NGC 1052, NGC 1209, and NGC 6758, we identified the extended emission lines $\text{H}\beta$, $[\text{O III}]\lambda 4959\text{\AA}$ and/or $[\text{O III}]\lambda 5007\text{\AA}$. For NGC 6861, we only measured

emission at $H\beta$ for its nuclear aperture spectrum ($r \leq 1$ arcsec). For IC 5328 only, no previous work had identified these lines (e.g. Donzelli & Pastoriza 1997), probably because the lines are very weak and the stellar contribution had not been adequately considered. From these galaxies, only IC 5328 and NGC 6861 did not have a classification in the literature for their gas emission.

Emission line diagnostic diagrams have been extensively used to distinguish among $H\text{II}$ regions (photoionization by stars), AGN, and LINER natures. The most widely adopted method is based on the BPT diagnostic diagrams proposed by Baldwin et al. (1981), which utilizes line ratios such as $[\text{O III}]\lambda 5007\text{\AA}/H\beta$ versus $[\text{N II}]\lambda 6584\text{\AA}$ lines/ $H\alpha$ and $[\text{O III}]\lambda 5007\text{\AA}/H\beta$ versus $[\text{S II}]\lambda 6717$ 6731\AA lines/ $H\alpha$. Unfortunately, we were not able to use this type of diagnostic diagrams because the spectral coverage of our data does not extend up to the region of $H\alpha$ and $[\text{N II}]\lambda 6584\text{\AA}$ lines.

An alternative diagram using stellar mass Mass-Excitation (MEx) diagnostic diagrams proposed by Juneau et al. (2011, 2014) combines $[\text{O III}]\lambda 5007\text{\AA}/H\beta$ and the stellar mass and successfully distinguishes between star formation and AGN emission. This MEx diagnostic diagram can be used to classify the ionization source of IC 5328, NGC 1052, NGC 1209, and NGC 6758, since we measured the $[\text{O III}]\lambda 5007\text{\AA}/H\beta$ ratio.

The MEx diagram has the advantage of requiring $[\text{O III}]\lambda 5007\text{\AA}/H\beta$ emission line ratio and, therefore, is suitable for our cases. Fig. 10 shows this diagram for our sample of objects. The stellar mass was estimated by the equation given by Juneau et al. (2011), which was established by relating the stellar masses derived from SED fitting and rest-frame K-band absolute magnitudes.

As can be seen in this figure, all galaxies occupy the AGN region. To better assess the classes of the AGNs, we used the code given by Juneau et al. (2011), and calculated the probability that the galaxies belong to the following classes: star-forming, composite (mixed star-formation, and AGN), LINER, and Seyfert 2. According to Juneau et al. (2011), this probabilistic AGN classification scheme has a built-in uncertainty, but this is useful to utilize in combination with other alternative diagrams, for which the classification is not certain. We found that IC 5328, NGC 1052, NGC 1209, and NGC 6758 are probably LINER.

5. Discussion

One of the open questions about the formation and evolution of massive early-type galaxies, even under the paradigm of hierarchical formation scenario, is which main factor plays a determinant role: the progenitor mass or the environment (the known debate “nature versus nurture”, e.g. Cooper et al. 2007; Tasca et al. 2009; Merlin et al. 2012). Specifically, the SFH, chemical evolution, and merger history of a given ETG are imprinted in the spatial distribution of their stellar populations.

The kinematics of stars and gas can also provide some clues about the more recent phase of the merger history of a massive ETG. It is also pertinent to investigate possible relations among the galaxy, the dynamical state, and the stellar population properties as well as between the stellar population properties and the stellar/gas kinematics (this analysis will be carry out in a future work).

The current sample of ETGs includes slow and fast rotators distributed over groups and pairs (3 out of 8 galaxies under possible interaction). Optical emission lines from ionized gas are in 5 out of 8 objects, with 3 of them already confirmed as LINERs in the literature. The sample galaxies also span non-negligible variations in total luminosity (1 mag in M_B) and nuclear velocity dispersion (about 0.3 dex). We found that the mean stellar age of the sample objects is 11.4 ± 1.3 Gyr. $[\text{M}/\text{H}]$ covers an interval of around 0.2 dex, $[\text{Fe}/\text{H}]$ changes in about 0.2 dex, and $[\alpha/\text{Fe}]$ ranges from the solar value up to +0.4 dex. Therefore, we can explore what the resulting stellar population properties means for the sample ETGs as a function of the nuclear stellar velocity dispersion in some sense, distinguishing the sample ETGs as group and pair galaxies, as interacting and non-interacting galaxies, and finally galaxies with or without warm gas emission.

We compiled our results about the spatial distribution of stellar population properties galaxy-by-galaxy in Sect. 4.1 and Sect. 4.3. Other individual characteristics collected from the literature, such as morphology, environment, presence/absence of emission lines, and interaction signature can be found in Appendix A.

We noticed some trends and correlations between light-weighted mean stellar population properties (quantified in the nucleus and inside one R_e) and the nuclear stellar velocity dispersion. All parameters

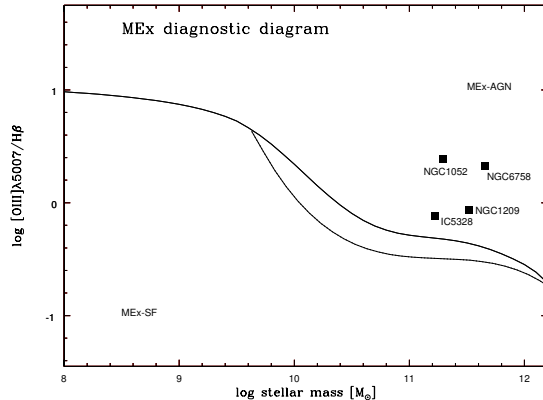


Fig. 10.— Stellar mass as a function of the line ratio $[\text{O III}]\lambda 5007\text{\AA}/\text{H}\beta$. The empirical curves were taken from Juneau et al. (2014) and the upper mark is the main division between star forming galaxies from AGN. The region between the two empirical curves contains a mix of star forming galaxies and AGN.

are dealt with in the logarithm scale. Nuclear velocity dispersion (measurements corrected by the aperture effect and homogenized collected from HYPERLEDA⁵ database (Makarov et al. 2014): is directly related to the mass inside a circular radius of 813 pc (Coma normalization, Jorgensen et al. 1995) and indirectly quantifies the total mass of the galaxy.

A positive trend exists between $\log(\text{age})$ and $\log(\sigma_v^0)$ for the region inside $1 R_e$ only, i.e. more massive galaxies have older stars as also found by McDermid et al. (2015) and Trager et al. (2000b,a) (see Fig. 11). There is also a positive correlation between the integrated $[\text{M}/\text{H}]$ inside one R_e and velocity dispersion, but this correlation is also erased for the nuclear $[\text{M}/\text{H}]$ ($r \leq 1$ arcsec); see Fig. 12. Our results also prove the well-known correlation between α -enhancement and velocity dispersion. We obtained positive correlations between them for both estimates of $[\alpha/\text{Fe}]$ (nuclear and integrated in $1 R_e$); reported in Fig. 13. Finally, the ETGs of our sample follow a strong positive correlation between the radial gradient of $[\text{M}/\text{H}]$ (scale $\text{dex}/R/R_e$) and $\log(\sigma_v^0)$, such that more massive galaxies have shallower gradients or even null gradients in metallicity (see Fig. 14). Although this relation has a high linear correlation coefficient ($r = 0.762$), we suppose that some bias effect is involved, especially because we would expect the opposite as quantified by González Delgado et al. (2015) and Kuntschner et al. (2010), who noticed that the stellar

metallicity gradient is roughly dependent on the stellar mass M_\odot , up to around $10^{11} M_\odot$. Perhaps, one reason is that we are dealing with only luminous ETGs in sparse groups and interacting pairs.

Our results corroborate the stellar population analysis of the CALIFA survey from (González Delgado et al. 2015) that included 40 ellipticals (E0-E7) and 32 lenticular (S0) nearby galaxies, which was also carried out with STARLIGHT. The CALIFA observations show that massive ellipticals exhibit negative mass-weighted metallicity radial gradients, similar to what we detected in luminosity-weighted metallicity (CALIFA gradients were measured up to almost three effective radius in the case of Es). This CALIFA analysis confirms that ellipticals are composed of older and more metal rich stellar populations than spirals at fixed total stellar mass M_* , in agreement with our results. It indicates that the star formation quenching does not only depend on the galaxy mass, but also on the morphology. We obtained flat radial profiles of age in our sample of ETGs, in agreement with CALIFA results (Martín-Navarro et al. 2018), which found rather flat age and $[\text{Mg}/\text{Fe}]$ radial gradients, weakly dependent on the effective velocity dispersion of the galaxy within half-light radius.

Furthermore, we found for this sample of ETGs no distinction between the radial gradients of stellar population properties in ETGs in sparse groups and ETGs in interacting pairs. **This result agrees with**

⁵<http://leda.univ-lyon1.fr/>

that found by Goddard et al. (2017), who studied the internal radial gradients of stellar population properties within $1.5 R_e$ and analysed the impact of galaxy environment, using a representative sample of 721 galaxies. These authors suggested that galaxy mass is the main driver of stellar population gradients in both early and late-type galaxies, and any environmental dependence, if present at all, must be very subtle.

Additionally, we detected in three of the sample ETGs (IC 5328, NGC 6758, and NGC 5812) the presence of intermediate-young and intermediate-old populations. Moreover, using the MEx diagnostic diagram, we verified the LINER emission in IC 5328, NGC 1052, NGC 1209, and NGC 6758, and no correlation was found between the stellar population properties and the LINER presence.

6. Summary and Conclusions

This work presents detailed results about stellar populations properties in the region up to one R_e in a sample of eight massive nearby ETGs; all but one are members of sparse groups (three of them in pairs under possible interaction and other three in pairs with weak interaction). Five galaxies are classified as ellipticals (IC 5328, NGC 1052, NGC 1209, NGC 5812, and NGC 7507), two are simultaneously classified as ellipticals and giant ellipticals (NGC 6758 and NGC 7796) and one as lenticular (NGC 6861). Five of them (IC5328, NGC1052, NGC1209, NGC6861, and NGC6758) have LINER nuclei, such that all sample galaxies have $M_B < M_B^*$ at $z = 0$. Long-slit spectra at $\lambda\lambda 320-6360 \text{ \AA}$ were analysed across both apparent photometric axes, when possible.

The regions up to one effective radius of all sample galaxies are basically dominated by alpha-enhanced metal-rich old stellar populations, likely due to rapid star formation episodes that induced efficient chemical enrichments. On average, the age and $[\alpha/\text{Fe}]$ gradients are null, and the $[\text{M}/\text{H}]$ gradients are negative, although discordant cases were found splitting the galaxies with common characteristics in three groups as listed ahead. We found no correlation between the stellar population properties and the LINER presence as well as between the stellar properties and environment or gravitational interaction, suggesting that the influence of progenitor mass can not be discarded in the formation and

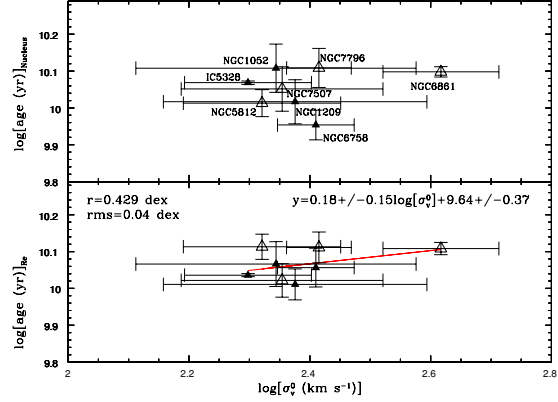


Fig. 11.— $\log(\text{age})_{\text{Nucleus}}$ and $\log(\text{age})_{R_e}$ versus $\log(\sigma_v^0)$. ETGs are denoted by triangles. The ones that harbour LINER nuclei are plotted with filled triangles. A simple lsq fit is represented by a solid red line, only when the linear correlation coefficient r exceeds 0.400. A two-sigma clipping is also adopted to exclude outliers. The derived linear correlation is shown in the right top corner, and the fit r and rms are in the left top corner, in the case when the fit r is greater than 0.400.

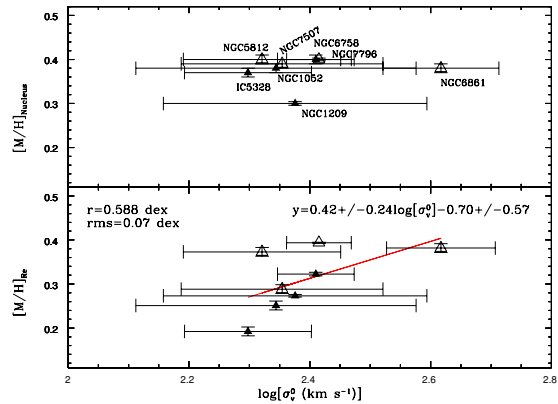


Fig. 12.— $[\text{M}/\text{H}]_{\text{Nucleus}}$ and $[\text{M}/\text{H}]_{R_e}$ versus $\log(\sigma_v^0)$. Same notation as Figure 11.

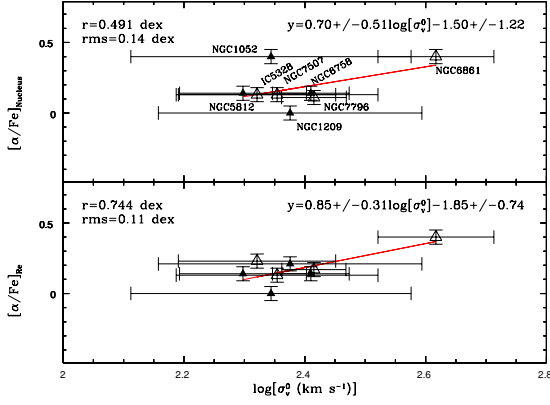


Fig. 13.— $[\alpha/\text{Fe}]_{\text{Nucleus}}$ and $[\alpha/\text{Fe}]_{R_e}$ versus $\log(\sigma_v^0)$. Same notation as Figure 11.

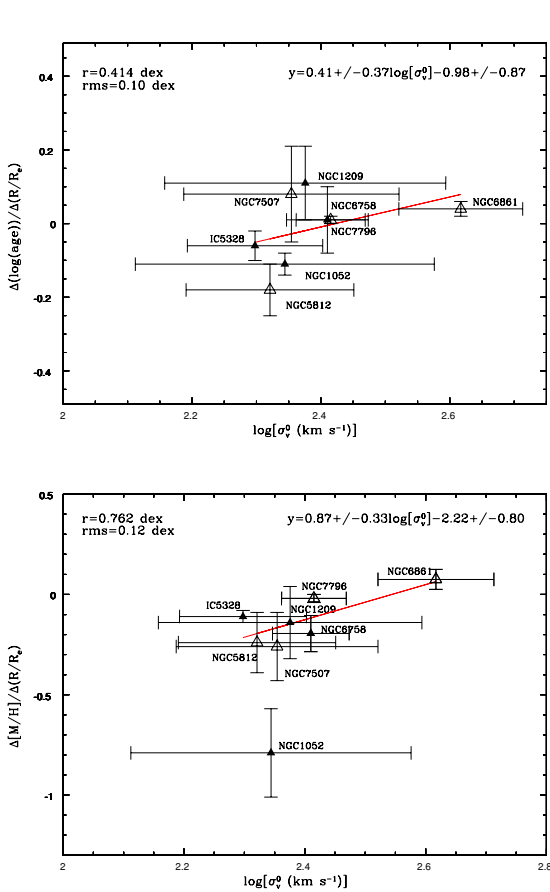


Fig. 14.— Age $(\Delta(\log(\text{age}))/\Delta(R/R_e))$ and metallicity $(\Delta[M/H]/\Delta(R/R_e))$ radial gradients versus $\log(\sigma_v^0)$. Same notation as Figure 11.

evolution of massive ETGs.

Our results on the stellar population synthesis approach and warm ionized gas are summarily presented as follows.

1. The results of stellar population synthesis, split the galaxies into: (i) IC 5328 and NGC 1052 that have some stellar properties in common as described, (ii) NGC 1209 being the only one with a positive $[\alpha/\text{Fe}]$ gradient, and (iii) NGC 5812, NGC 6758, NGC 6861, NGC 7507, and NGC 7796, which have uniform old metal-rich stellar populations in the observed regions in terms of derived age and chemical composition indicating a rapid star formation with a strong and fast chemical enrichment. A common stellar property is that all sample galaxies are dominated by old stellar populations ($8 \times 10^9 < t \leq 13 \times 10^9$ years). IC 5328 and NGC 1052 both have a negative gradient of metallicity that changes in the over-solar regime. While IC 5328 has a $[\text{Fe}/\text{H}]$ negative gradient, NGC 1052 has a positive one. Specifically, NGC 1052 and NGC 1209 have variable $[\alpha/\text{Fe}]$ (decreased outwards for NGC 1052 and crescent outwards for NGC 1209). IC 5328, NGC 5812, NGC 6758, NGC 7507, and NGC 7796 have homogeneous moderate α -enhancement ($[\alpha/\text{Fe}] = +0.2$ dex), and NGC 6861 has homogeneous high α -enhancement ($[\alpha/\text{Fe}] = +0.4$ dex). The stellar population synthesis detected contributions greater than 20 percent (flux scale) of intermediate-young populations in IC 5328 and NGC 6758 (age between 1 and 4 Gyr) as well as contributions of intermediate-old populations in NGC 5812 (4 – 8 Gyr). IC 5328 and NGC 5812 are galaxies in distinct pairs under possible interaction (both pairs inside groups) and NGC 6758 is galaxy in a group.

2. Concerning the detection of ionized gas, we can state that extended gas is present in IC 5328, NGC 1052, NGC 1209, and NGC 6758. The greatest radial extension of this emitting gas is across the major axis of NGC 6758, reaching a radial distance of $0.4 R_e$. NGC 6861 likely owns a very concentrated nuclear ionized gas emission. The presence of a LINER is identified in IC 5328, NGC 1052, NGC 1209, and NGC 6758.

Our results on stellar populations properties (up to $0.5 R_e$) and ionized gas (up to $0.4 R_e$), empirically characterize luminous ETGs, which were selected from nearby pairs and sparse groups including interacting galaxies and LINERs. These results add detailed information to recover the SFH and chemical enrichment imprinted in the stellar populations of each individual galaxy as well as to investigate the influence of galaxy mass, environment, interaction with other galaxy and AGN feedback in the galaxy formation and evolution.

Acknowledgements

D. A. Rosa is grateful for the scholarship from CAPES and CNPq foundations for the PCI/MCTIC/INPE posdoc fellowship, (process 300082/2016 – 9). A. Milone and I. Rodrigues thank the Brazilian foundation CNPq/MCTIC (grants number 309562/2015 – 5, 311920/2015 – 2, respectively). A. Krabbe thanks FAPESP (grant number 2016/21532 – 9). We all acknowledge the usage of the HyperLeda database (<http://leda.univ-lyon1.fr>). This research made use of the NASA/IPAC Extragalactic Database (NED), which is operated by the Jet Propulsion Laboratory, California Institute of Technology, under contract with the National Aeronautics and Space Administration. IRAF is written and supported by the National Optical Astronomy Observatories (NOAO) in Tucson, Arizona. NOAO is operated by the Association of Universities for Research in Astronomy (AURA), Inc. under cooperative agreement with the National Science Foundation.

REFERENCES

- Annibali, F., Bressan, A., Rampazzo, R., Zeilinger, W. W., & Danese, L. 2007, *A&A*, 463, 455
- Annibali, F., Bressan, A., Rampazzo, R., et al. 2010, *A&A*, 519, A40
- Asari, N. V., Cid Fernandes, R., Stasińska, G., et al. 2007, *MNRAS*, 381, 263
- Baldwin, J. A., Phillips, M. M., & Terlevich, R. 1981, *PASP*, 93, 5
- Baumgartner, W. H., Tueller, J., Markwardt, C. B., et al. 2013, *ApJS*, 207, 19
- Bertin, G., Bertola, F., Buson, L. M., et al. 1994, *A&A*, 292, 381
- Bettoni, D., Galletta, G., & García-Burillo, S. 2003, *A&A*, 405, 5
- Binney, J., & Tremaine, S. 2008, *Galactic Dynamics: Second Edition* (Princeton University Press)
- Cardelli, J. A., Clayton, G. C., & Mathis, J. S. 1989, *ApJ*, 345, 245
- Carlberg, R. G. 1984a, *ApJ*
- . 1984b, *ApJ*
- Carollo, C. M., Danziger, I. J., & Buson, L. 1993, *MNRAS*, 265, 553
- Caso, J. P., Richtler, T., Bassino, L. P., et al. 2013, *A&A*, 555, A56
- Cid Fernandes, R., Asari, N. V., Sodr e, L., et al. 2007, *MNRAS*, 375, L16
- Cid Fernandes, R., Gu, Q., Melnick, J., et al. 2004, *MNRAS*, 355, 273
- Cid Fernandes, R., Mateus, A., Sodr e, L., Stasińska, G., & Gomes, J. M. 2005, *MNRAS*, 358, 363
- Cooper, M. C., Newman, J. A., Coil, A. L., et al. 2007, *MNRAS*, 376, 1445
- Cox, D. P. 1972, *ApJ*, 178, 159
- Croton, D. J., Springel, V., White, S. D. M., et al. 2006, *MNRAS*, 365, 11
- da Costa, L. N., Willmer, C. N. A., Pellegrini, P. S., et al. 1998, *AJ*, 116, 1
- Damjanov, I., Abraham, R. G., Glazebrook, K., et al. 2011, *ApJ*, 739, L44
- De Lucia, G., Springel, V., White, S. D. M., Croton, D., & Kauffmann, G. 2006, *MNRAS*, 366, 499
- de Vaucouleurs, G., de Vaucouleurs, A., Corwin, Jr., H. G., et al. 1991, *S&T*, 82, 621
- Donzelli, C. J., & Pastoriza, M. G. 1997, *ApJS*, 111, 181
- Driver, S., & De Propris, R. 2003, *Ap&SS*, 285, 175
- Escudero, C. G., Faifer, F. R., Bassino, L. P., Calder n, J. P., & Caso, J. P. 2015, *MNRAS*, 449, 612

- Feldmann, R., Quataert, E., Hopkins, P. F., Faucher-Giguère, C.-A., & Kereš, D. 2017, *MNRAS*, 470, 1050
- Ferré-Mateu, A., Vazdekis, A., & de la Rosa, I. G. 2013, *MNRAS*, 431, 440
- Ferreiro, D. L., & Pastoriza, M. G. 2004, *A&A*, 428, 837
- Ferreiro, D. L., Pastoriza, M. G., & Rickes, M. 2008, *A&A*, 481, 645
- Giuricin, G., Marinoni, C., Ceriani, L., & Pisani, A. 2000, *ApJ*, 543, 178
- Goddard, D., Thomas, D., Maraston, C., et al. 2017, *MNRAS*, 465, 688
- González Delgado, R. M., García-Benito, R., Pérez, E., et al. 2015, *A&A*, 581, A103
- Gonzalez-Martin, O., Diaz-González, D., Acosta-Pulido, J., et al. 2014, in *The X-ray Universe 2014*, 84
- Hernández-García, L., González-Martín, O., Márquez, I., & Masegosa, J. 2013, *A&A*, 556, A47
- Hirschmann, M., Naab, T., Ostriker, J. P., et al. 2015, *MNRAS*, 449, 528
- Ho, L. C., Filippenko, A. V., & Sargent, W. L. W. 1997, *ApJS*, 112, 315
- Howell, J. H. 2005, *AJ*, 130, 2065
- Huang, S., Ho, L. C., Peng, C. Y., Li, Z.-Y., & Barth, A. J. 2016, *ApJ*, 821, 114
- Idiart, T. P., Silk, J., & de Freitas Pacheco, J. A. 2007, *MNRAS*, 381, 1711
- Jorgensen, I., Franx, M., & Kjaergaard, P. 1995, *MNRAS*, 276, 1341
- Juneau, S., Dickinson, M., Alexander, D. M., & Salim, S. 2011, *ApJ*, 736, 104
- Juneau, S., Bournaud, F., Charlot, S., et al. 2014, *ApJ*, 788, 88
- Kobayashi, C. 2004, *MNRAS*, 347, 740
- Koprolin, W., & Zeilinger, W. W. 2000, *A&AS*, 145, 71
- Kuntschner, H., Emsellem, E., Bacon, R., et al. 2010, *MNRAS*, 408, 97
- Lane, R. R., Salinas, R., & Richtler, T. 2015, *A&A*, 574, A93
- Larson, R. B. 1974, *MNRAS*, 166, 585
- . 1975, *MNRAS*, 173, 671
- Lauberts, A., & Valentijn, E. A. 1989, *The Messenger*, 56, 31
- Lauer, T. R. 1985, *MNRAS*, 216, 429
- Li, Z., Han, Z., & Zhang, F. 2007, *A&A*, 464, 853
- Liske, J., Lemon, D. J., Driver, S. P., Cross, N. J. G., & Couch, W. J. 2003, *MNRAS*, 344, 307
- Longhetti, M., Rampazzo, R., Bressan, A., & Chiosi, C. 1998, *A&AS*, 130, 267
- Macchetto, F., Pastoriza, M., Caon, N., et al. 1996, *A&AS*, 120, 463
- Machacek, M. E., O’Sullivan, E., Randall, S. W., Jones, C., & Forman, W. R. 2010, *ApJ*, 711, 1316
- Makarov, D., Prugniel, P., Terekhova, N., Courtois, H., & Vauglin, I. 2014, *A&A*, 570, A13
- Maoz, D., Nagar, N. M., Falcke, H., & Wilson, A. S. 2005, *ApJ*, 625, 699
- Martín-Navarro, I., Vazdekis, A., Falcón-Barroso, J., et al. 2018, *MNRAS*, 475, 3700
- Mason, R. E., Rodríguez-Ardila, A., Martins, L., et al. 2015, *ApJS*, 217, 13
- Mateus, A., Sodr e, L., Cid Fernandes, R., et al. 2006, *MNRAS*, 370, 721
- McDermid, R. M., Alatalo, K., Blitz, L., et al. 2015, *VizieR Online Data Catalog*, 744
- Merlin, E., Chiosi, C., Piovani, L., et al. 2012, *MNRAS*, 427, 1530
- Michard, R., & Prugniel, P. 2004, *A&A*, 423, 833
- Mihos, J. C., & Hernquist, L. 1996, *ApJ*, 464, 641
- Milone, A. D. C., Rickes, M. G., & Pastoriza, M. G. 2007, *A&A*, 469, 89
- Naab, T., & Burkert, A. 2003, *ApJ*, 597, 893

- Obreja, A., Domínguez-Tenreiro, R., Brook, C., et al. 2013, *ApJ*, 763, 26
- Oser, L., Ostriker, J. P., Naab, T., Johansson, P. H., & Burkert, A. 2010, *ApJ*, 725, 2312
- Panuzzo, P., Rampazzo, R., Bressan, A., et al. 2011, *A&A*, 528, A10
- Papovich, C., Labbé, I., Quadri, R., et al. 2015, *ApJ*, 803, 26
- Paturel, G., Fang, Y., Petit, C., Garnier, R., & Rousseau, J. 2000, *A&AS*, 146, 19
- Phillips, M. M., Jenkins, C. R., Dopita, M. A., Sadler, E. M., & Binette, L. 1986, *AJ*, 91, 1062
- Pierce, M., Brodie, J. P., Forbes, D. A., et al. 2005, *MNRAS*, 358, 419
- Raimann, D., Storchi-Bergmann, T., Bica, E., & Alloin, D. 2001, *MNRAS*, 324, 1087
- Raimann, D., Storchi-Bergmann, T., Quintana, H., Hunstead, R., & Wisotzki, L. 2005, *MNRAS*, 364, 1239
- Ramos Almeida, C., Bessiere, P. S., Tadhunter, C. N., et al. 2012, *MNRAS*, 419, 687
- Rampazzo, R., Annibali, F., Bressan, A., et al. 2005, *A&A*, 433, 497
- Rembold, S. B., Pastoriza, M. G., Ducati, J. R., Rubio, M., & Roth, M. 2002, *A&A*, 391, 531
- Richtler, T., Salinas, R., Lane, R. R., Hilker, M., & Schirmer, M. 2015, *A&A*, 574, A21
- Rosa, D. A., Dors, O. L., Krabbe, A. C., et al. 2014, *MNRAS*, 444, 2005
- Salinas, R., Richtler, T., Bassino, L. P., Romanowsky, A. J., & Schuberth, Y. 2012, *A&A*, 538, A87
- Sánchez, S. F., Rosales-Ortega, F. F., Iglesias-Páramo, J., et al. 2014, *A&A*, 563, A49
- Sánchez-Blázquez, P., Gorgas, J., Cardiel, N., & González, J. J. 2006a, *A&A*, 457, 787
- . 2006b, *A&A*, 457, 809
- Sansom, A. E., de Castro Milone, A., Vazdekis, A., & Sánchez-Blázquez, P. 2013, *MNRAS*, 435, 952
- Sansom, A. E., Hibbard, J. E., & Schweizer, F. 2000, *AJ*, 120, 1946
- Santini, P., Fontana, A., Grazian, A., et al. 2009, *A&A*, 504, 751
- Schlafly, E. F., & Finkbeiner, D. P. 2011, *ApJ*, 737, 103
- Simien, F., & Prugniel, P. 1997, *A&AS*, 126, doi:10.1051/aas:1997279
- Stark, D. P., Ellis, R. S., Bunker, A., et al. 2009, *ApJ*, 697, 1493
- Tal, T., van Dokkum, P. G., Nelan, J., & Bezanson, R. 2009, *AJ*, 138, 1417
- Tasca, L. A. M., Kneib, J.-P., Iovino, A., et al. 2009, *A&A*, 503, 379
- Terlevich, A. I., & Forbes, D. A. 2002, *MNRAS*, 330, 547
- Thomas, D., Maraston, C., Bender, R., & Mendes de Oliveira, C. 2005, *ApJ*, 621, 673
- Trager, S. C., Faber, S. M., Worthey, G., & González, J. J. 2000a, *AJ*, 120, 165
- . 2000b, *AJ*, 119, 1645
- van den Bosch, R. C. E., Gebhardt, K., Gültekin, K., Yıldırım, A., & Walsh, J. L. 2015, *ApJS*, 218, 10
- van Gorkom, J. H. 2004, *Clusters of Galaxies: Probes of Cosmological Structure and Galaxy Evolution*, 305
- van Gorkom, J. H., Knapp, G. R., Raimond, E., Faber, S. M., & Gallagher, J. S. 1986, *AJ*, 91, 791
- Vazdekis, A., Coelho, P., Cassisi, S., et al. 2015, *MNRAS*, 449, 1177
- Vermeulen, R. C., Ros, E., Kellermann, K. I., et al. 2003, *A&A*, 401, 113
- Weinmann, S. M., Kauffmann, G., van den Bosch, F. C., et al. 2009, *MNRAS*, 394, 1213
- Yamada, T., Kodama, T., Akiyama, M., et al. 2005, *ApJ*, 634, 861
- Zirm, A. W., Stanford, S. A., Postman, M., et al. 2008, *ApJ*, 680, 224

This 2-column preprint was prepared with the AAS L^AT_EX macros v5.2.

A. The early-type galaxies sample

IC 5328 is an E4 galaxy, member of a sparse group, with a total of four galaxies based on our criteria (see Section 2), in which IC 5328 is the unique ETG. It is the main galaxy of the closest pair of our sample, along with IC 5328 A, at a projected distance of 8.2 kpc. IC 5328 A is a SB galaxy, much smaller than IC 5328 with a pure exponential brightness profile. It shows clear signs of tidal interaction (Ferreiro & Pastoriza 2004) and weak emissions in H α and [N II] lines possibly due to two identified H II regions (Donzelli & Pastoriza 1997; Ferreiro & Pastoriza 2004; Ferreiro et al. 2008). IC 5328 is a globally dynamic hot system, but the stars show slow rotation around a minor axis. Its stellar velocity dispersion profile exhibits irregularities (as observed by Longhetti et al. 1998), possibly indicating the presence of a dynamical double core. We have not found any work relating to radial gradients of stellar population properties for this galaxy.

NGC 1052 is a LINER E4 galaxy and the third brightest member of the sparse group NOGG 165 with eleven galaxies in total as identified by Giuricin et al. (2000) (NOGG: Nearby Optical Galaxy Group), whose brightest galaxy is NGC988 (SB), or with twelve galaxies according to our criteria. There are only two ETGs in this group. This LINER in particular shows variability in the ultraviolet (Maoz et al. 2005), near-infrared (Mason et al. 2015), radio (Vermeulen et al. 2003), and X-ray (Hernández-García et al. 2013). Many other works have confirmed the presence of emission lines in the optical and mid-infrared. Recently, Gonzalez-Martin et al. (2014), using an X-ray catalogue with 40 LINERs, figured out that this galaxy seems to be more like a Seyfert than a LINER. Its stellar kinematics along both photometric axes has been extensively measured by several works; van den Bosch et al. (2015) is an example. Tidal tails have been identified in NGC 1052 as interaction sign (van Gorkom et al. 1986; Sansom et al. 2000). Its closest companion is 2MASX J02413514-0810243, which makes with NGC 1052 a weak pair, according to our criteria (see Sec. 2).

NGC 1209 is an E6? galaxy in a weak pair with NGC 1231 (Sc), based on our criterion. However, Giuricin et al. (2000) identified it in a E+E pair with NGC 1199 (E3) (which seems to be the central galaxy of a compact group), NGC 1209 being the brightest one (NOGG 183). Annibali et al. (2010) and Panuzzo et al. (2011) supposed that NGC 1209 is a LINER based on optical and mid-infrared emission lines. Ramos Almeida et al. (2012) revealed evidence of disturbed elliptical morphology in NGC 1209 at relatively high surface brightness levels by investigating the effects of galaxy interactions in the triggering of powerful radio galaxies (PRGs), which are likely the result of past or on-going gravitational interaction. Tal et al. (2009) identified X-like isophotal structure and a NW linear feature as tidal signatures. We found stellar kinematics measurements across major photometric axis for **NGC 1209** indicating that elliptical is a fast rotator (Carollo et al. 1993; Simien & Prugniel 1997).

NGC 5812 is an E0 galaxy in the group NOGG 849, which contains three galaxies (Giuricin et al. 2000), and is the brightest member and the only ETG. However, according to our criteria it belongs to a sparse group of six galaxies. The closest companion is IC 1084, in a projected distance of 38.2 kpc. An interacting signature was found in NGC 5812, i.e. a tidal tail due to a gravitational interacting with a dwarf companion (Tal et al. 2009). No emission lines in the optical and mid-infrared have been detected in the spectrum of NGC 5812 (Annibali et al. 2010; Panuzzo et al. 2011). Its stellar kinematics was first quantified by Bertin et al. (1994) across a single direction. Following our criteria, NGC 5812 is member of a sparse group and makes a pair with IC 1084.

NGC 6758 is an E+ (late-type elliptical) or cD galaxy. It is, the sixth brightest member of a group with 22 or 30 galaxies (Giuricin et al. 2000), the NOGG 940 group, whose brightest galaxy is IC 4837 A. This galaxy is a LINER host (Annibali et al. 2010; Machacek et al. 2010). However, according to our criteria, it belongs to a sparse group of seven galaxies in total, with no physical companion. The galaxy shows some evidence of past interaction (Escudero et al. 2015; Machacek et al. 2010). Its stellar kinematics in NGC 6758 has been analysed by several works. We consider NGC 6758 as a sparse group member.

NGC 6861 is a SA0^{-s} galaxy in the NOGG 962 group with 10 members and is, the second brightest galaxy (the brightest is NGC 6868) (Giuricin et al. 2000). According to our criteria, it belongs to a sparse group of 17 galaxies, making a weak pair with IC 4943; although Chandra X-ray observations reveal that NGC 6861 probably undergoes an on-going interaction with NGC 6868 that could induce a merger between two sub-structures of the group in a near future (Machacek et al. 2010). Optical emission lines from warm gas have already been measured in the spectrum of this galaxy (Phillips et al. 1986; Macchetto et al. 1996). However, there is no classification for this emission yet. Its

stellar kinematics was, for instance, investigated by Koprolin & Zeilinger (2000), and classified as a fast rotator. We consider NGC 6861 as a sparse group member in a weak pair.

NGC 7507 is an E0 galaxy in a sparse group with seven members in total based on our criterion, under possible interaction with GALEXASC J231146.81-283145.2. There are no clear signs of tidal distortions in NGC 7507 (Caso et al. 2013), although photometric shells have been identified (Tal et al. 2009; Ramos Almeida et al. 2012) and a moderately high index of peculiarity Σ_2 has been measured (Michard & Prugniel 2004). It also has two stellar haloes with opposite small rotations confirmed as a S+S merger remnant (Lane et al. 2015; Salinas et al. 2012). Its stellar kinematics suggests it is a slow rotator. Bettoni et al. (2003) did not compile ionized gas emission for the galaxy. We consider NGC 7507 as an interacting pair galaxy in a sparse group.

NGC 7796 is a cD galaxy that is isolated, based on our criteria, although it has NGC 7796 1 as a dwarf satellite, which exhibits a tidal tail and multiple nuclei (Richtler et al. 2015). On the other hand, there is no photometric interaction sign in NGC 7796 (Rembold et al. 2002). Macchetto et al. (1996) did not measure optical emission lines for NGC 7796. Several works quantified the stellar kinematics of **NGC 7796** across different directions. We consider NGC 7796 as a field galaxy.

B. Radial gradients of stellar population properties analysed galaxy-by-galaxy

For **NGC 5328**, the age and global metallicity radial distributions across both photometric axes of IC 5328 are shown in Fig. 5. While we found a flat age gradient across major axis and a nearly flat age gradient across minor axis (providing a uniform age of about 12 ± 1 Gyr), the metallicity gradient is negative across both axes (-0.36 ± 0.10 dex/ (R/R_e) for major axis and -0.52 ± 0.19 dex/ (R/R_e) for minor axis) indicating a nuclear over-solar global metallicity ($[M/H] = +0.32$ dex) and a decrease of around $\sim +0.2$ dex up to about $0.4 R/R_e$. The integrated age and metallicity inside one R_e (quantified across major axis only) are about 11 Gyr and $[M/H] = +0.20$ dex, respectively, which are in agreement with their radial variations within the observational errors.

For **NGC 1052**, the age and global metallicity radial distributions across major axis are shown in Fig. 6. The radial gradients of both parameters are negatives (see Table 4), with the metallicity gradient the steepest of all sample galaxies. However the change in age from the nucleus up to about $0.3 R/R_e$ is still compatible with a constant value (13 ± 1 Gyr downing up to 12 ± 1 Gyr). The metallicity changes from $[M/H] = +0.42$ dex at the nucleus downing up to $[M/H] = +0.17$ dex (a decrease of 0.25 dex that is seven times greater than the average error of 0.04 dex). The integrated age and metallicity inside one R_e are about 12 Gyr and $[M/H] = +0.25$ dex, respectively, which are in agreement with their radial variations within the observational errors.

For **NGC 1209**, the age and global metallicity radial distributions across major axis are shown in Fig. 7. The radial gradients of both parameters are compatible with zero, taking into account their errors that are equal or greater than their gradient values (see Table 4). Age and $[M/H]$ from the nucleus up to about $0.23 R/R_e$ change around constant values (11 ± 1 Gyr and $+0.27 \pm 0.03$ dex). The integrated age and metallicity inside one R_e are about 10 ± 1 Gyr and $Z = +0.27 \pm 0.01$ dex, respectively, which are in agreement with their radial variations within the observational errors.

For **NGC 5812**, the age and global metallicity radial distributions across EW direction are shown in Fig. 6. The radial gradients of both parameters are negative (see Table 4). However, the change in age from the nucleus up to about $0.27 R/R_e$ is still compatible with a constant value (13 ± 1 Gyr downing up to 12 ± 1 Gyr). The metallicity changes from $[M/H] = +0.41$ dex at the nucleus downing up to $[M/H] = +0.34$ dex (a decrease of 0.07 dex that is 2 times greater the average error of 0.03 dex). The integrated age and metallicity inside one R_e are about 13 Gyr and $[M/H] = +0.37$ dex, respectively, which are in agreement with their radial variations within the observational errors.

For **NGC 6758**, the age and global metallicity radial distributions across major and minor axes are shown in Fig. 6. The radial gradients of both parameters are compatible with zero, taking into account their errors that are equal or greater than their gradient values (see Table 4). In fact, age and $[M/H]$ from the nucleus up to about $0.32 R/R_e$ change around constant values (12 ± 1 Gyr and $+0.32 \pm 0.01$ dex). The integrated age and metallicity inside one R_e are about 11 ± 1 Gyr and $[M/H] = +0.322 \pm 0.004$ dex, respectively, which are in agreement with their radial variations within the observational errors (note that population synthesis over the one R_e region was only applied by using the major axis data).

For **NGC 6861**, the age and global metallicity radial distributions across major and minor axes are shown in Fig. 7. The radial gradients of both parameters are null over the major axis and positive over the minor axis (see Table 4). However, the change in age across minor axis from the nucleus up to about $0.3 R/R_e$ is still compatible with a constant value (variation smaller than 0.3 Gyr !). The age and $[M/H]$ change across the major axis are around 13 Gyr and $[M/H]= +0.40$ dex (from the nucleus up to $0.52 R/R_e$), respectively. Over the minor axis, the metallicity changes from $[M/H]= +0.36$ dex at the nucleus downing up to $[M/H]= +0.40$ dex (an increase of 0.06 dex that is 2 times greater than the average error of 0.02 dex). The integrated age and metallicity inside one R_e are about 13 Gyr and $[M/H]= +0.38$ dex, respectively, which are in agreement with their radial variations within the observational errors (note that population synthesis over the one R_e region was only applied by using the major axis data).

For **NGC 7507**, the age and global metallicity radial distributions across EW direction are shown in Fig. 8. While we have found a flat age gradient providing a uniform age of about 12 ± 1 Gyr, the metallicity gradient is negative (-0.46 ± 0.39 dex/ (R/R_e)) despite its great error, pointing to a nuclear over-solar global metallicity ($[M/H]= +0.41$ dex) that decreases down to about $[M/H]= +0.28$ dex at $0.15 R/R_e$ (a variation of 0.13 dex that is still greater than the metallicity error). The integrated age and metallicity inside one R_e are about 10.5 Gyr and $[M/H]= +0.29$ dex, respectively, which are in agreement with their radial variations within the observational errors.

For **NGC 7796**, the age and global metallicity radial distributions across major and minor axes are shown in Fig. 8. The radial gradients of both parameters are compatible with zero, taking into account the radial variations of age and metallicity themselves and the gradient errors that are comparable with the own gradient values (see Table 4), even though the metallicity gradient is slightly negative (but supplying a very small variation of 0.05 dex in $[M/H]$). Age and $[M/H]$ from the nucleus up to about $0.3 R/R_e$ (major axis) and $0.2 R/R_e$ change around constant values (13 ± 1 Gyr and $+0.40 \pm 0.01$ dex). The integrated age and metallicity inside one R_e are about 10 ± 1 Gyr and $[M/H]= +0.40 \pm 0.01$ dex, respectively, which are in agreement with their radial variations (note that population synthesis over the one R_e region was only applied by using the major axis data).

C. Stellar population synthesis

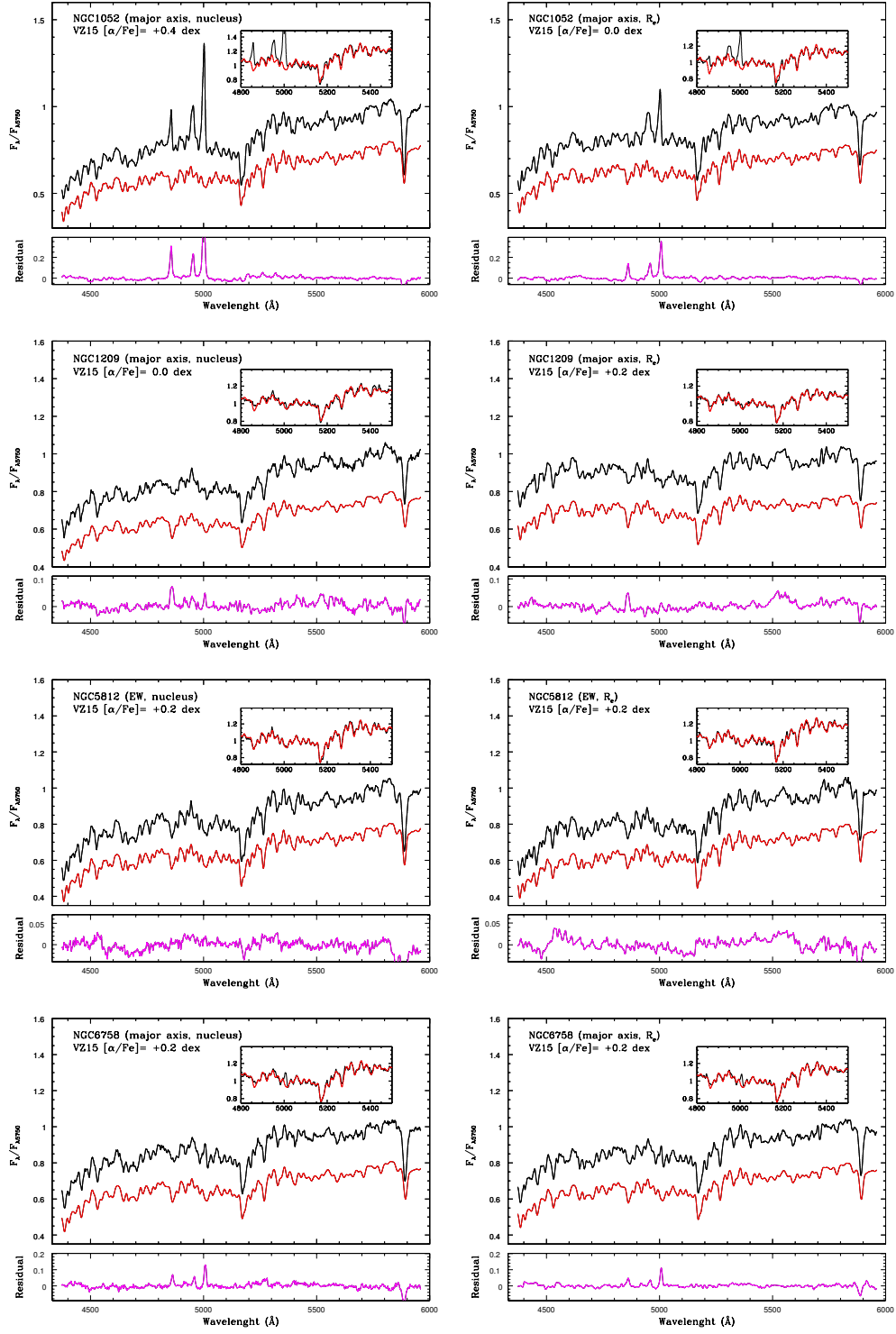


Fig. 15.— Stellar population synthesis for the nuclear (left panel) and one R_e (right panel) regions across the major axis of IC 5328, NGC 1052, NGC 1209, NGC 5812, and NGC 6758 (Notation as in Fig. 2).

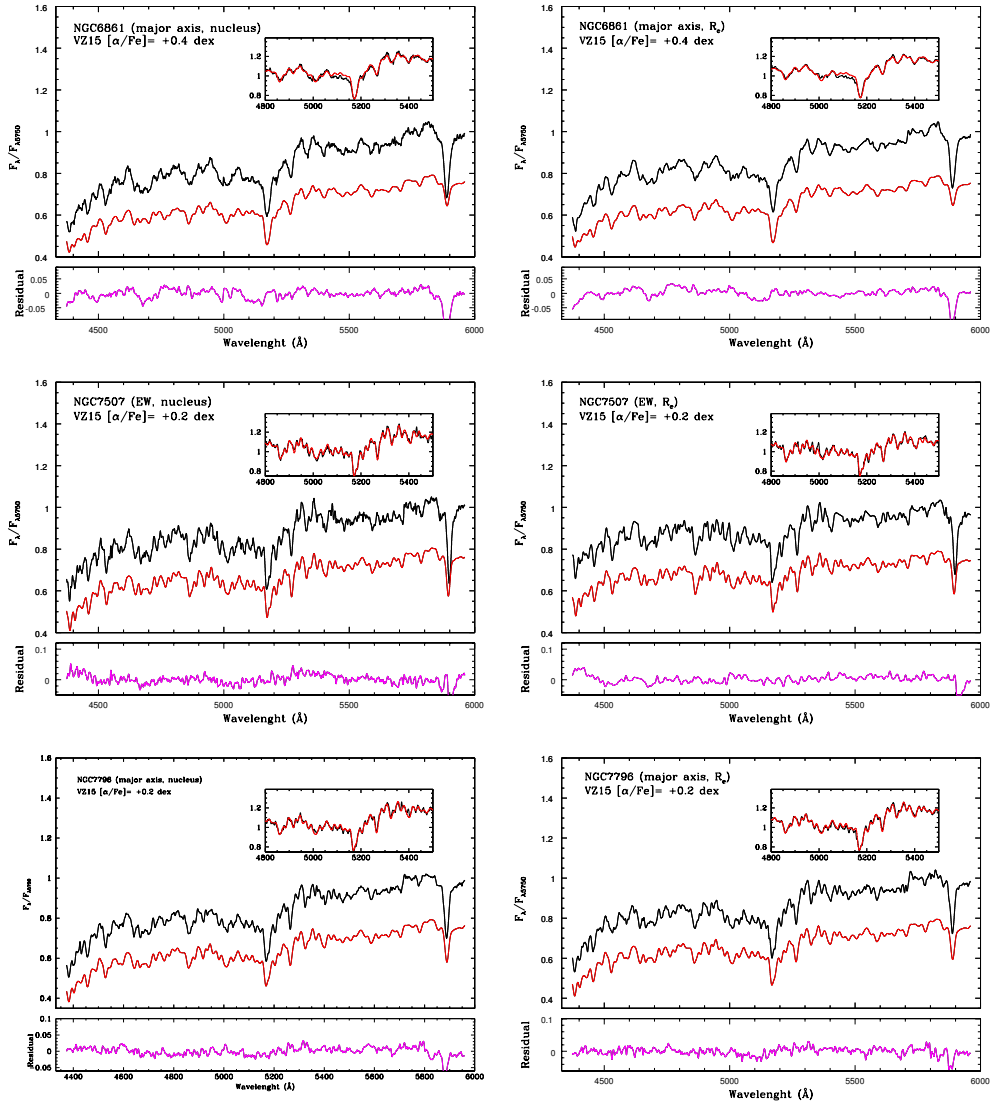


Fig. 16.— The same as Fig. 15, but for NGC 6861, NGC 7507, and NGC 7796.

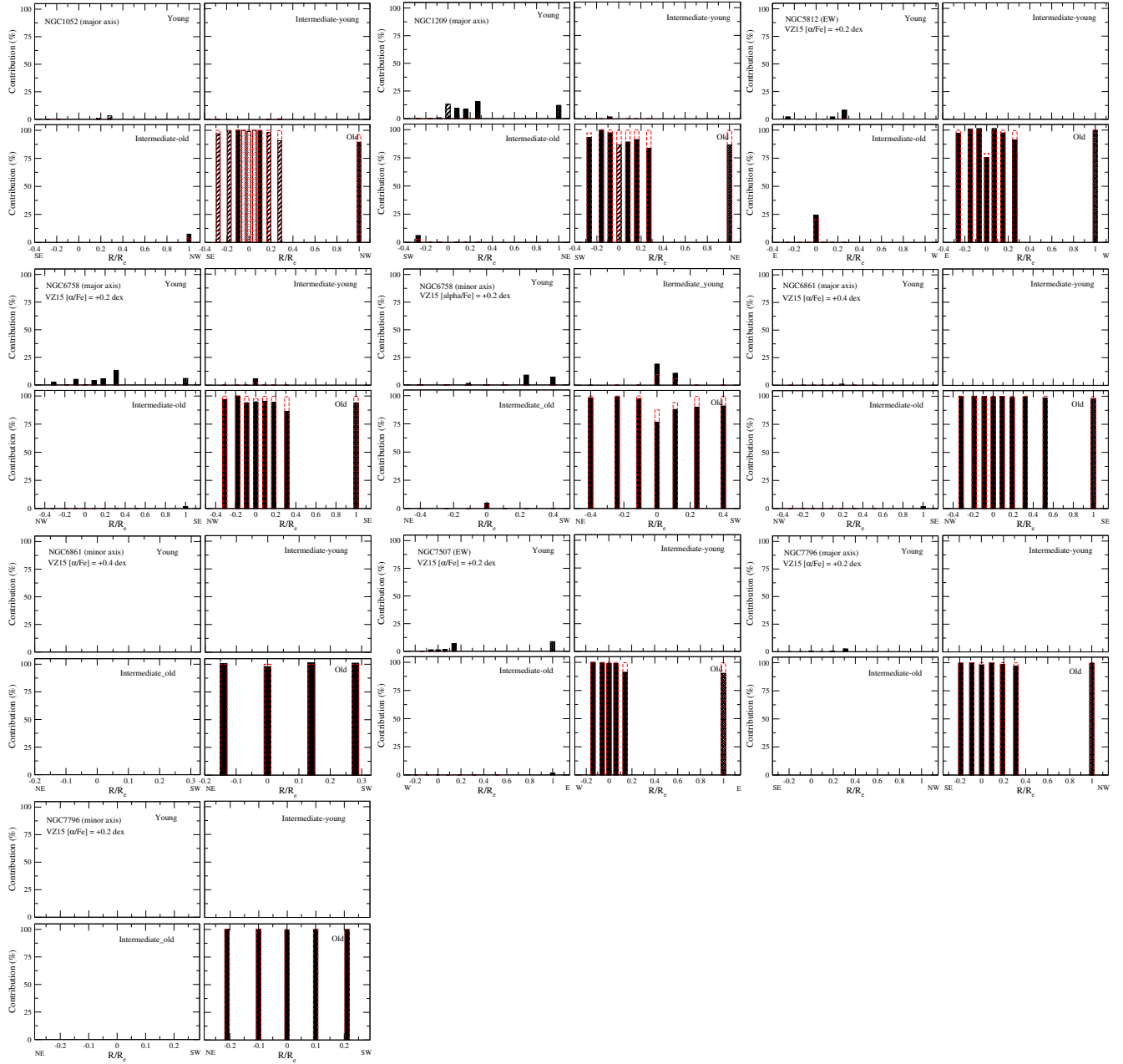


Fig. 17.— Same as Fig. 3, but for NGC 1052, NGC 1209, NGC 6758, NGC 6861, and NGC 7796 on the photometric axes and EW for NGC 5812, and NGC 7507.

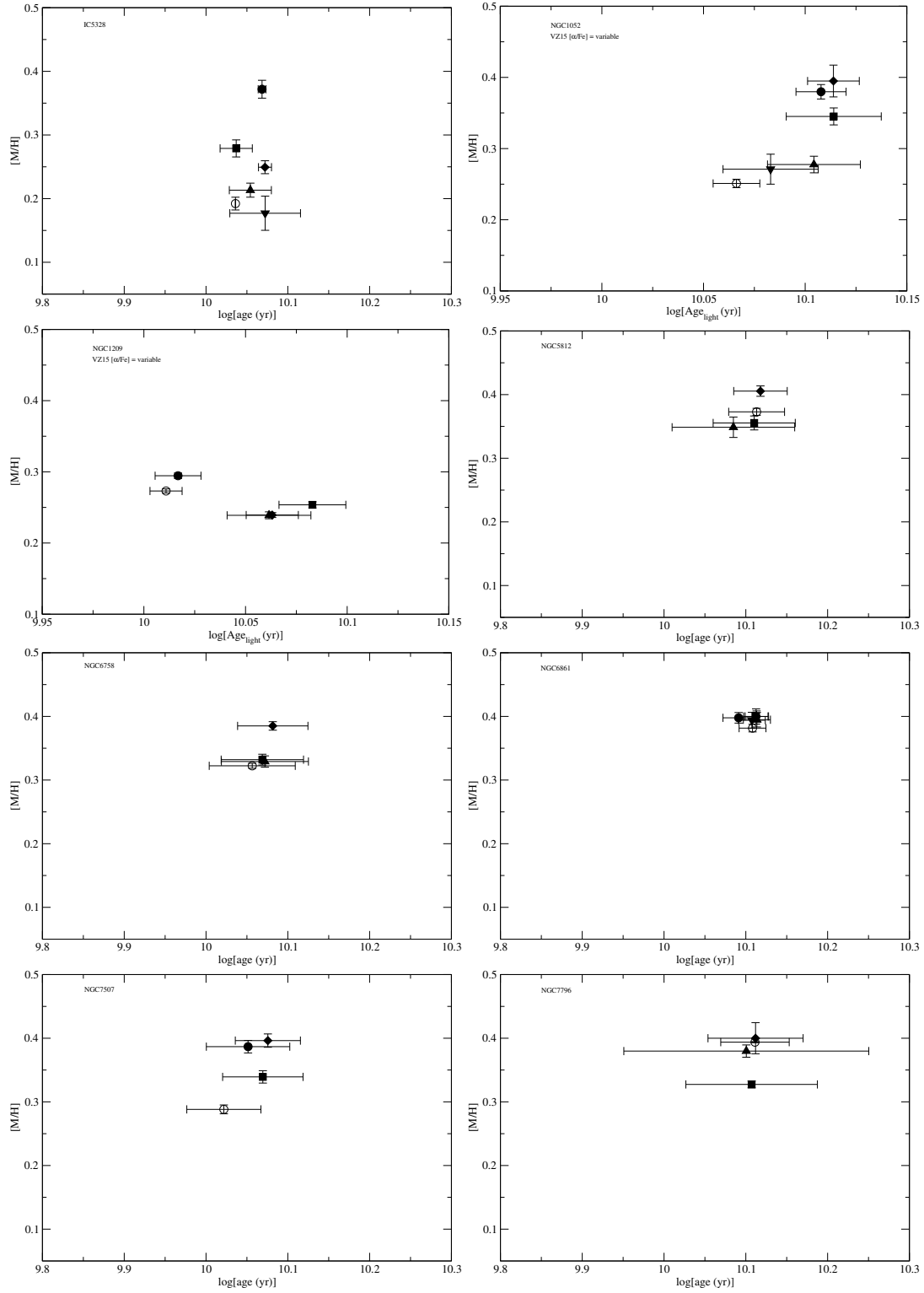


Fig. 18.— Same as Fig. 9, but for six sample galaxies separately shown as indicated (stellar population synthesis results across a single slit direction: major axis for IC 5328, NGC 6758, NGC 6861, and NGC 7796, and EW for NGC 5812 and NGC 7507).